The spectrum of persistent volcanic flank instability: A review and proposed framework based on Kīlauea, Piton de la Fournaise, and Etna

Michael P. Poland, Aline Peltier, Alessandro Bonforte, Giuseppe Puglisi

The spectrum of persistent volcanic flank instability: A review and proposed framework based on Kīlauea, Piton de la Fournaise, and Etna

Michael P. Poland*[1], Aline Peltier[2], Alessandro Bonforte[3], Giuseppe Puglisi[3]

1 U.S. Geological Survey
Cascades Volcano Observatory
1300 SE Cardinal Ct., Suite 100
Vancouver, WA 98683 USA
Tel: +1 360-993-8906
mpoland@usgs.gov

2 Institut de Physique du Globe de Paris, Sorbonne Paris Cité
Observatoire Volcanologique du Piton de la Fournaise
Univ. Paris Diderot, UMR 7154 CNRS, F-97418 La plaine des Cafres, France

3 Istituto Nazionale di Geofisica e Vulcanologia
Sezione di Catania
Osservatorio Etneo, Catania 95125, Italy

* Corresponding Author

Abstract

Persistent motion of the south flank of Kīlauea Volcano, Hawai‘i, has been known for several decades, but has only recently been identified at other large basaltic volcanoes—namely Piton de la Fournaise (La Réunion) and Etna (Sicily)—thanks to the advent of space geodetic techniques. Nevertheless, understanding of long-term flank instability is based largely on the

example of Kīlauea, despite the large differences in the manifestations and mechanisms of the process when viewed through a comparative lens. For example, the rate of flank motion at Kīlauea is several times that of Etna and Piton de la Fournaise and is accommodated on a slip plane several km deeper than is probably present at the other two volcanoes. Gravitational spreading also appears to be the dominant driving force at Kīlauea, given the long-term steady motion of the volcano's south flank regardless of eruptive/intrusive activity, whereas magmatic activity plays a larger role in flank deformation at Etna and Piton de la Fournaise. Kīlauea and Etna, however, are both characterized by heavily faulted flanks, while Piton de la Fournaise shows little evidence for flank faulting. A helpful means of understanding the spectrum of persistent flank motion at large basaltic edifices may be through a framework defined on one hand by magmatic activity (which encompasses both magma supply and edifice size), and on the other hand by the structural setting of the volcano (especially the characteristics of the subvolcanic basement or subhorizontal intravolcanic weak zones). A volcano's size and magmatic activity will dictate the extent to which gravitational and magmatic forces can drive motion of an unstable flank (and possibly the level of faulting of that flank), while the volcano's structural setting governs whether or not a plane of weakness exists beneath or within the edifice and can facilitate flank slip. Considering persistent flank instability using this conceptual model is an alternative to using a single volcano as a "type example"—especially given that the example is usually Kīlauea, which defines an extreme end of the spectrum—and can provide a basis for understanding why flank motion may or may not exist on other large basaltic volcanoes worldwide.

Keywords: flank instability; deformation; basaltic volcanism; Kīlauea; Etna; Piton de la Fournaise

1. Introduction

Volcanic flank instability is clearly an important process in the evolution of large basaltic volcanoes, but its manifestations and mechanisms are poorly known because insights are drawn mostly from the example of Hawai'i. This lack of depth stems from the fact that flank motion has only been recognized as an important process since the mid-20th century, so opportunities for study, especially outside Hawai'i, have been limited. Indeed, space-based geodetic techniques—

especially Global Navigation Satellite Systems (GNSS) and Interferometric Synthetic Aperture Radar (InSAR)—that evolved during the late 20th century played a key role in defining the extent, rate and pattern of flank instability at many volcanoes [e.g., Owen et al, 1995; Bonforte and Puglisi, 2003, González et al., 2010; Brenguier et al., 2012]. It is therefore important to ask the questions of how and why flank motion varies between volcanoes, and how current knowledge may be exploited to increase understanding of the process at volcanoes worldwide.

In 1964, James Moore, then a geologist with the U.S. Geological Survey's Hawaiian Volcano Observatory, authored two manuscripts that were the first to provide evidence of instability in large basaltic volcanoes. In the first article, Moore and Krivoy [1964] proposed that the south flank of Kīlauea was sliding seaward due to gravity and pressurization of the volcano's East Rift Zone, based on deformation and structures associated with eruptive activity in 1962. About a decade later, the postulated seaward motion was confirmed by trilateration measurements, leading subsequent authors to posit that a large earthquake might be possible due to flank compression [Swanson et al., 1976]—a prescient hypothesis, since an M7.7 earthquake occurred in 1975 (while the trilateration results were in press). In the second paper, Moore [1964] suggested that bathymetric data from the sea floor north of the Hawaiian islands of O'ahu and Moloka'i recorded the presence of massive landslides. This possibility was debated for several decades, until comprehensive mapping of the sea floor around Hawai'i settled the matter and demonstrated beyond any doubt that massive landslides were a common process in the archipelago [Moore et al., 1989].

In the more than half-century since Moore's recognition of the various forms of instability in Hawai'i, flank motion and catastrophic failures have been identified at numerous large basaltic volcanoes around the world. At Piton de la Fournaise (La Réunion Island), for example, large-scale debris avalanches have been identified offshore from marine data and have been interpreted as resulting from flank collapses [e.g. Lénat et al., 1990; Oehler et al., 2008; Le Friant et al., 2011] and gravitationally driven volcanic spreading [e.g. Oehler et al., 2005; Michon and Saint- Ange, 2008]. Indeed, more than 500 km^3 of avalanche deposits cover the eastern submarine flank of the volcano [e.g. Oehler et al., 2005]. In Sicily, the continental margin off the eastern coast of Etna shows an offset due to a large bulge that is characterized by several semi-circular steps, interpreted as evidence of large landslides and suggesting gravitational instability of the submarine base of the edifice and extending onto the volcano's subaerial eastern

flank [Borgia et al., 1992; Rust and Neri, 1996; Chiocci et al., 2011; Azzaro et al., 2013]. Evidence for varying degrees of flank instability has also been found on many other basaltic volcanoes, such as the Canary Islands [Holcomb and Searle, 1991; Urgeles et al., 1997; Carracedo et al., 1999; Hürlimann et al., 2000; Krastel et al., 2001; Masson et al., 2002], Galápagos [Geist et al., 2002], and Tristan de Cunha [Holcomb and Searle, 1991].

Flank instability is so ubiquitous that it is surprising when it is not found at a large volcano, motivating investigators to ask the question "why not?" [e.g., Nakamura, 1980; Geist et al., 2006]. A growing body of research is now emphasizing the importance of flank instability on the evolution of large basaltic volcanoes, and also on the hazards posed by those volcanoes [e.g., Denlinger and Morgan, 2014]. Unstable flanks not only experience large earthquakes, but can also fail catastrophically, resulting in large subaerial and/or submarine landslides that, for island or coastal volcanoes, can trigger tsunami. In addition, flank instability and eruptive activity feed off one another. Flank motion can promote eruptive activity, eruptive activity results in gravitational loading and oversteepening, and repeated rift zone intrusions and pressurization of a magmatic system have the ability to "push" a flank closer to some sort of failure.

Despite the widespread nature of flank instability on large basaltic volcanoes, the mechanisms and manifestations of the process are diverse; therefore, it would be a mistake to universally apply models developed at any specific volcano. For example, Hawai‘i, despite being the type locality for instability of large basaltic volcanoes, is a poor analog for the Galápagos in terms of flank behavior [e.g., Poland, 2014a]. In an effort to better define the spectrum of flank instability at large basaltic edifices, we review the process at three well studied but vastly different volcanoes: Kīlauea, Piton de la Fournaise, and Etna (Fig. 1). We chose these sites because they are among the best-monitored and most active volcanoes in the world, and also because they represent extremes across the spectrum of basaltic volcanism in terms of their sizes and tectonic settings. As such, these three volcanoes provide excellent examples upon which to define a conceptual framework for flank processes.

Here, we focus on ongoing, deep-seated, persistent flank motion (sometimes referred to as "volcanic spreading" [Borgia et al., 1992; Merle and Borgia, 1996]) that can be characterized by geological study and geophysical techniques. We do not explore other styles of flank motion, including large-scale catastrophic collapse, which has never been witnessed and thus remains a poorly understood process [e.g., Iverson, 1995]; shallow motion of surficial deposits, which may

be correlated with magmatic activity, as at Stromboli, Italy [Di Traglia et al., 2014]; nor transient co-eruptive motion that may be associated with sector collapse at arc volcanoes, as exemplified by the May 2010 deformation observed at Pacaya, Guatemala [Schaefer et al., 2015, 2016]. Through a comparative analysis of Kīlauea, Piton de la Fournaise, and Etna—three volcanoes commonly used as type examples for large basaltic edifices [e.g., Michon et al., 2015; Peltier et al., 2015a]—we find that the style and magnitude of long-term persistent instability scale with the size of the host volcanic system and the character of the volcanic substrate. This general framework may be useful for better understanding flank instability at other large basaltic volcanoes that are not as well characterized as these three sites.

2. Geological characteristics and eruptive activity of example volcanoes

2.1 Kilauea

Kīlauea is the youngest and currently the most active volcano on the Island of Hawai‘i, located in the middle of the Pacific Plate at the leading edge of a ~6000-km-long chain of islands and seamounts that marks the activity of the Hawaiian hot spot over the past 70 million years [Clague and Dalrymple, 1987; Tilling and Dvorak, 1993; Clague and Sherrod, 2014]. Given that the volcano overlaps significantly with its much larger neighbor, Mauna Loa, Kīlauea's volume is difficult to determine, having been variously estimated to range between 31,600 km^3 [Robinson and Eakins, 2006] and 11,000 km^3 [Lipman and Calvert, 2013] (Table 1). The inception age of Kīlauea is probably no earlier than 275 ka, although the vigorous shield-building tholeiitic stage of volcanism probably did not begin until about 100 ka [Lipman and Calvert, 2013]. Magma supply to the volcano since the 1950s appears to have averaged approximately 0.1 km^3/yr as estimated from rates of magma storage and eruption, although geophysical and geochemical monitoring data from the 2000s have documented both a surge and a lull, suggesting that years-long variations in supply can and do occur [Poland et al., 2012; Poland, 2014b; Anderson and Poland, 2016]. Variability in magma supply over centuries has also been proposed as an explanation for cycles of effusive and explosive volcanism at Kīlauea [Swanson et al., 2014].

Structurally, Kīlauea can be broadly described as hosting a summit caldera and two rift zones (Fig. 2). The summit caldera is ephemeral, experiencing cycles of formation and filling over the past several thousand years that may be tied to variations in magma supply over time

[Swanson et al., 2014]. Geophysical data currently support the presence of at least two magma storage areas beneath Kīlauea's summit—one at ~1.5 km beneath the center of the caldera, and a second (the primary magma storage area for the volcano) about 3 km beneath the south part of the caldera [e.g., Poland et al., 2014]. Kīlauea's two rift zones radiate away from the summit to the east and southwest. There is some evidence that each rift zone is actually comprised of two parts at different depths that connect to the shallower and deeper summit magma storage areas [Poland et al., 2014]. The rift systems provide a means for lateral magma transport from the summit to the distal flanks of the volcano, where magma may be stored in small reservoirs within the rift zones or erupted at the surface. The deep rift zones, below about 3 km depth, show evidence of steady opening [Delaney et al., 1990; Owen et al., 1995, 2000a], perhaps driven by the presence of dense cumulates [Clague and Denlinger, 1994].

In addition to the caldera and rift zones, Kīlauea hosts two normal fault systems, both of which trend ENE-WSW, which is the dominant structural grain of the volcano [Johnson et al., 2015] (Fig. 2). The Koa'e Fault System, comprised of mostly north-facing normal faults, links the East and Southwest Rift Zones south of the caldera and has been a site of occasional magmatic intrusions [Poland et al., 2014, and references therein]. The Hilina Fault System is made up of south-facing normal faults along the volcano's southern coast and is associated with instability of that flank [Cannon and Bürgmann, 2001; Cannon et al., 2001; Denlinger and Morgan, 2014], having last ruptured during the 1975 M7.7 Kalapana earthquake [Lipman et al., 1985].

Eruptive activity at Kīlauea alternates between centuries-long periods of lava effusion and centuries-long periods of explosive eruptions [Swanson et al., 2014]. Since the early 1800s, eruptions have been mostly effusive from the summit and both rift zones. East Rift Zone eruptive activity has been nearly continuous since the onset of the Pu'u 'Ō'ō eruption in 1983, and a coincident summit eruption, characterized by a persistent plume of ash and gas and an actively circulating lava lake, has been ongoing since 2008 [Orr et al., 2015].

2.2 Piton de la Fournaise

Piton de la Fournaise is a hot spot intra-plate basaltic shield volcano located on La Réunion Island (Indian Ocean) and is the active surface expression of the 5000-km-long hot spot chain that originated with the Deccan Trap flood basalt 65 million years ago [Duncan, 1981;

Morgan, 1981]. The volcano began erupting before 500 ka [Gillot and Nativel, 1989] on the eastern slope of the currently inactive Piton des Neiges edifice, the base of which lies 4 km below sea level on oceanic crust, and the shape of which controls the geometry of the island [Lefriant et al., 2011]. Piton de la Fournaise represents less than 3% of the volume of the island (which is estimated at ~50,100 km^3) [Villeneuve et al., 2014]. The volcano is dominated by the ~13 × 9 km Enclos Fouqué caldera, which is approximately 4500 years old and includes a terminal cone cut by two summit craters (Dolomieu and Bory; Fig. 3). The formation of the Enclos Fouqué structure is controversial; four different models have been proposed: 1) polyphase caldera collapse at the top of the structure accompanied by lateral eastward sliding [Bachèlery, 1981]; 2) a single giant landslide [Labazuy, 1996; Oehler et al., 2004]; 3) lateral eastward motion that triggered vertical collapse of the summit area [Merle and Lénat, 2003]; and 4) downward drag related to a dense intrusive complex located 1 km below the eastern part of the structure [Michon and Saint-Ange, 2008]. Excluding subtle lineaments highlighted on Digital Elevation Models [Michon and Saint-Ange, 2008] and the scars of the Osmonde paleo-river (Fig. 3), no fault scarps are visible in the landscape.

Geochemical and geophysical data suggest the presence of several intermittently connected magma reservoirs between the near surface and ~11 km below the summit [e.g. Battaglia et al., 2005; Peltier et al., 2009; Brenguier et al., 2012; Got et al., 2013; Di Muro et al., 2014]. The shallowest reservoir, from which most of the dikes feeding recent eruptions have initiated, is located about 1.5–2 km depth below the summit craters [e.g. Peltier et al., 2007, 2008; Prôno et al., 2009].

Three rift zones, oriented N10°−25° (northeast rift zone), N160°−180° (southeast rift zone), and N120°, start from the summit and extend outside the Enclos Fouqué caldera (Fig. 3) [Michon et al., 2007; Bonali et al., 2011; Saint- Ange et al., 2013]. The northeast and southeast rift zones are arcuate, whereas the N120° rift zone is linear. The extension of the N120° rift zone from the summit cone to the east is limited to the lower eastern slopes of the volcano, but to the west it extends at least 15 km. Eruptive activity on the NW branch of the N120° rift zone is not common, with a repeat interval of ~200 years over the last 30,000 years [e.g. Michon et al., 2015]. Based on the distribution of eruptive fissures, pit craters, and cinder cones, Michon et al. [2007, 2015] distinguish between upper and lower parts of the rift zones, defining “summit” and “outer” segments, although the precise geometry of Piton de la Fournaise rift zones and their

connectivity are still debated [Michon et al., 2007; Bonali et al., 2011; Saint-Ange et al., 2013]. In contrast to Kīlauea, no permanent magma storage has been detected beneath or within Piton de la Fournaise rift zones, which appear to only represent zones of weakness that mark preferred paths for magmatic intrusions (particularly the northeast and southeast rift zones) and that bound the mobile seaward eastern flank.

Although some phreatic and phreatomagmatic eruptions have been reported historically [e.g. Peltier et al., 2012, Michon et al., 2013], eruptive activity over the past ~200 years has been mostly effusive, with lava fountains and flows. Since the 18th century, 97% of all eruptions have occurred within the Enclos Fouqué caldera [Villeneuve and Bachèlery, 2006], with eruptive fissures opening either inside the summit Dolomieu crater (summit eruptions) or along one of the rift zones (proximal and distal eruptions, the latter being located more than 5 km from the summit) [Peltier et al., 2009; Roult et al., 2012].

Since the Observatoire Volcanologique du Piton de la Fournaise (OVPF/IPGP) was established in 1980, Piton de la Fournaise has erupted an average of 2–3 times per year, with mean eruptive volumes of 8×10^6 m^3 [e.g. Peltier et al., 2009; Roult et al., 2012]. The magma supply rate to the volcano has been estimated at 0.01–0.04 km^3/yr (Table 1) on the basis of excess crustal thickness [White, 1993] and recent eruption rate [Peltier et al., 2009].

2.3 Etna

Mount Etna, the highest active volcano in Europe (3340 m above sea level as of summer 2007 [Bisson et al., 2016]), is a basaltic stratovolcano in eastern Sicily (Italy). The volcano is located in a complex tectonic setting due to the convergence of the African and European plates and also experiences flank instability [Lentini et al., 2006; Branca et al., 2011]. Etna is at the front of the Apennine-Maghrebian Chain on its northern and western sides, borders the northern portion of Malta Escarpment (the Mesozoic continental margin) on its eastern side, and overlies clayish-sandy Pliocene-Pleistocene Catania-Gela foredeep deposits on its southern side. The eastern coastline of Etna is cut by the Timpe system of normal faults, which are responsible for seismicity on the lower eastern flank of the volcano (Fig. 4) [Azzaro, 2004; Barreca et al., 2013; Azzaro et al., 2013].

Volcanism in the Etna region has been occurring for about 500,000 years, with scattered eruptions from submarine fissures evolving to central vent activity from polygenetic centers. The

first transitional basaltic products clearly related to the earliest stages of the current stratovolcano began erupting at about 200 ka. The present Mongibello cone, marking the summit of the volcano, grew following the formation of a caldera at 15 ka. About 10 ka, the structure of the volcano was radically modified by slope failures that involved a large portion of the eastern flank and produced the wide depression of the Valle del Bove [Calvari et al, 2004; Branca et al., 2011]. The overall volume of the Etna edifice is difficult to assess, owing to uncertain knowledge of the volcano's basement; it has been estimated at 684 km^3 assuming a basal plane at sea level [Bisson et al., 2016]. Volcanic activity at Mt. Etna is characterized by frequent effusive eruptions accompanied by persistent Strombolian activity and lava fountains with occasional sub-Plinian eruptions, as indicated by both the historical and stratigraphic records [Branca and Del Carlo 2004; Del Carlo et al., 2004]. Eruptions occur at or close to the summit craters (summit eruptions), along flank fissures radiating from the summit sometimes to low elevations (flank eruptions), and rarely from magma ascent paths that are independent of the volcano's main conduit (eccentric eruptions). A higher density of eruptive fissures occur on the northeast and south flanks, defining the NE and S rifts, while a wide area of eruptive vents on the west flank marks the less prominent W rift. Since 1750 C.E., Etna has experienced an average of 2–3 flank eruptions every 25 years, but a sharp increase in this rate occurred after 1975 [Branca and Del Carlo, 2004]. The past few decades have been characterized by periods of continuous recharge, interrupted by lateral and summit eruptions. Harris et al. [2011, 2012] compiled and calculated erupted volumes during 1980–2010 and found an average eruption rate of about 0.8 m^3/s (0.025 km^3/yr). Allard et al. [2006] estimated a similar eruption rate (0.02 km^3/yr for the 1993–2005 period) but demonstrated from SO_2 emissions that 3-4 times more magma is degassing and stored than erupted, suggesting a magma supply rate of about 0.075 km^3/yr (Table 1). Since 2000, eruptive activity has been characterized by more frequent mild explosive activity, with hundreds of episodes of lava fountaining at the summit craters, mostly from the SE crater and a new vent in the vicinity [Acocella et al., 2016].

Geophysical data suggest that magma ascends beneath the western side of the volcano, but no magma chamber has been detected [Laigle et al., 2000; Patanè et al., 2003; Bonforte et al., 2008]. Seismic tomography studies have imaged a high-velocity and mainly aseismic volume beneath the southeastern part of the volcano, vertically extending from sea level downwards, which has been interpreted as a rigid body composed of magmatic intrusions. All pressure

sources modeled from ground deformation data are located along the northwestern border of this body, defining an almost vertical path ranging from 9 to 2–3 km depth that projects at the surface on the upper western flank of the volcano. The shallowest level of this range seems to mark the level of neutral buoyancy for magma, from where intrusions can follow the main conduit of the volcano towards the surface [Bonaccorso et al., 2011] or propagate as dikes away from the summit, for example, as was the case in 2001 [Puglisi et al., 2008]. Magma from the central conduit often intrudes radially along the two main rift zones on the upper southern and northeastern flanks (Fig. 4).

3. Characteristics of persistent flank instability at example volcanoes

Despite their differing sizes, tectonic settings, eruptive styles and histories, ages, and structures, Kīlauea, Piton de la Fournaise, and Etna are all affected to varying degrees by long-term persistent flank instability. Structures and deposits reflect this instability in some places, but the most obvious manifestation is current and ongoing surface deformation. Displacements at the surface are generally accommodated by motion on subsurface fault planes or ductile transition zones, but these are difficult to identify and constrain due to a lack of submarine deformation data and offshore structural information. Flank instability is also modulated to some extent by magmatic activity, and there is evidence for strong positive feedback between the two processes. Here, we examine surface deformation, flank structure, and interaction with magmatism in an effort to define the elements needed to construct a generalized conceptual framework of persistent flank instability at large basaltic volcanoes.

3.1 Deformation

At all three volcanoes, persistent ground deformation has been imaged in the form of subaerial seaward surface displacements measured by GNSS and InSAR. Motion is always on the unbuttressed sides of the volcanoes in the direction perpendicular to the bounding rift zones and involves motion towards the sea, but patterns of displacement vary in style between volcanoes (Fig. 5), which probably reflects differences in the structures that accommodate the deformation.

Seaward motion of Kīlauea's south flank was first documented by broad-scale trilateration surveys in the 1970s [Swanson et al., 1976], although instability was suspected from

structural studies and small-scale deformation measurements before that time [Moore and Krivoy, 1964]. The use of GNSS considerably elucidated understanding of flank displacements, providing a comprehensive four-dimensional perspective of surface motion [Owen et al., 1995, 2000a; Brooks et al., 2006]. The unstable flank is bounded to the north by Kīlauea's rift zones, the north sides of which are apparently stable (Fig. 5a) [Owen et al., 1995]. Seaward horizontal displacements south of the rift zones range from a few cm/yr on the south margins of the summit caldera and rift zones to ~8 cm/yr at the south coast [Owen et al., 2000a]. Vertical deformation at the summit and along the rift zones varies over time according to magmatic activity, but uplift characterizes the south coast (Fig. 5a, 6) [Owen et al., 2000a; Peltier et al., 2015a]. Although the south flank of the volcano is cut by the Hilina and Koa'e fault systems (Fig. 2), there is little evidence to suggest that these faults divide the flank into blocks that move independently between major earthquakes (modeling of InSAR data by Shirzaei et al. [2013] that argues such has yet to be confirmed by additional observations). Seaward flank motion is remarkably steady in time, at least since 1995, when continuous GNSS monitoring was initiated [Miklius et al., 2005]. The steady motion is interrupted by two processes (Fig. 6): 1) rift zone intrusions [e.g., Lundgren et al., 2013], which cause compression on the flank that may lead to strong earthquakes [Swanson et al., 1976; Poland et al., 2008], and 2) slow slip events (SSEs), which occur quasi-periodically and involve moment release equivalent to a ~M5–6 earthquake but spread over 24–48 hours, with minor accompanying seismicity [Cervelli et al., 2002a; Brooks et al., 2006; Segall et al., 2006; Wolfe et al., 2007; Montgomery-Brown et al., 2009, 2015].

At Piton de la Fournaise, even though eastward lateral spreading had long been suspected (based on the asymmetrical pattern of summit and near-summit deformation [e.g. Peltier et al., 2007, 2008; Derrien et al., 2015]), it was only confirmed in the mid-2000s, when up to 1.4 m of seaward motion was measured by InSAR on the volcano's east flank during the April 2007 distal eruption [e.g. Tinard, 2007; Clarke et al., 2013; Froger et al., 2015]. Unfortunately there were no permanent GNSS stations on the flank at the time of that eruption, so it is not possible to discriminate between cause and the consequence—in other words, are distal eruptions a consequence of seaward slip (Got et al., 2003), or is seaward slip a consequence of distal eruptions (e.g. Chaput et al., 2014; Froger et al., 2015)? Subsequent flank deformation, including during inter-eruptive periods, has been measured by systematic InSAR acquisitions (national monitoring system OI2, http://www.opgc.univ-bpclermont.fr/SO/televolc/volinsar/indexEN.php,

Clermont Ferrand University; CASOAR database) and six permanent GNSS stations, which were installed on the eastern flank of the volcano in 2009–2010 (via the ANR-08-RISK-011 UnderVolc project) (Fig. 5b) [Brenguier et al., 2012; Got et al., 2013; Peltier et al., 2015b]. Since they were established, four of the six permanent GNSS stations (located in the middle and southern part of the eastern flank) have recorded continuous eastward motion (of about 1.4 cm/yr) and subsidence (up to ~2.5 cm/yr) [Brenguier et al., 2012; Peltier et al., 2015b; Staudacher and Peltier, 2016]. Much of the subsidence is due to contraction of recent lava flows on which the stations are installed*;* the stations on the youngest lava flows have the greatest subsidence rates [Peltier et al., 2015b]. During the 2010–2014 inter-eruptive period, eastward velocities recorded on these four stations were quite similar (Fig. 5b). The two remaining GNSS stations, located in the northern part of the east flank, are decoupled from the others by paleostructures delimiting the Plaine des Osmondes collapse and Osmondes paleoriver (Fig. 3) [e.g. Courteaud, 1996; Michon and Saint-Ange, 2008] and did not record clear eastward motion, especially during inter-eruptive periods (< 3 mm/yr; Fig. 5b). Of these two stations, only the closest to the terminal cone recorded significant deformation during magmatic unrest in 2015. Seismicity on the eastern flank is sparse, with only a few low-magnitude events detected at about 2 km below sea level beneath the Grandes Pentes area (Fig. 3).

Like Piton de la Fournaise, Etna is characterized by eastward motion of its east flank (Fig. 5c). Starting in the 1990s, structural, geodetic and seismotectonic investigations suggested that a large portion of the eastern flank of Etna was sliding towards the sea [Borgia et al. 1992; Lo Giudice and Rasà, 1992; Patanè et al. 1994; McGuire et al. 1996; Rust and Neri 1996; Houliè et al., 2006]. During the 2000s, deformation measurements quantified the flank motion to have a mean rate of about 2–3 cm/yr, but with a maximum of about 3–5 cm/yr along the coast and northeast flank, variable in space and time [Solaro et al., 2010; Bonforte et al., 2011]. Localized SSEs have been identified in a few GPS stations, possibly related to the arrival of magmatic fluid in the edifice but not connected to any specific magmatic event (Mattia et al. 2015). Seismic and geodetic data indicate that the unstable flank is composed of several blocks with faults and fractures along their borders and that are characterized by distinct earthquake and displacement patterns [Bonforte and Puglisi, 2006; Solaro et al., 2010; Bonforte et al., 2011]. The northern boundary of the unstable sector is the Pernicana fault, which cuts the entire NE flank of the volcano from the NE rift zone to the sea (Fig. 4). The fault shows a mostly left-lateral mean slip

rate of about 2.5–3 cm/yr, but that rate can increase suddenly during magmatic events, when tens-of-cm-scale displacements and seismic swarms occur over the course of a few days [Bonforte et al., 2007a; Guglielmino et al., 2011; Ruch et al., 2013]. The rate of seaward flank motion decreases to the south across a number of faults with NNW-SSE and WNW-ESE trends [Azzaro et al., 2013; Barreca et al., 2013]. All faults on the southern slope of the volcano start from the south rift and continue to the sea, curving from a NNW-SSE azimuth with mostly normal motion on the upper slopes to an almost E-W orientation with mainly transcurrent kinematics at the coast [Bonforte et al., 2011]. The Trecastagni fault (Fig. 4) represents the main southern boundary of the sliding eastern sector [Gambino et al., 2011; Bonforte et al., 2011, 2013a], with reduced displacements across the southern slope of the volcano that are accommodated by other, less evident structures [Barreca et al., 2013; Bonforte et al., 2013b]. The entire southern sector of the volcano shows minor spreading motion, and the Ragalna fault (Fig. 4) represents the boundary of this sector on the southwest side of the volcano [Bonforte et al., 2011; Neri et al., 2007].

3.2 Flank structure

The structures of the mobile flanks on Kīlauea, Piton de la Fournaise, and Etna span the entire range of potential complexity, from a lack of exposed faults at the surface of Piton de la Fournaise, to the fault-bounded blocks of Etna. Unfortunately, the sliding surfaces that accommodate flank motion are poorly known in the cases of Etna and Piton de la Fournaise owing to a paucity of seismicity and a lack of deformation and structural data from the submarine flanks of the volcanoes.

At Kīlauea, the Koaʻe and the Hilina fault systems dominate the volcano's subaerial south flank. The depth of faulting in the Koaʻe is ambiguous, with evidence suggesting both shallow (upper several hundred meters) and deep (~10 km) extents [Duffield, 1975]. Initially, the depth of the Hilina faults was debated, with some workers speculating that the faults were the headwall of a large landslide [e.g., Morgan et al., 2000], while others argued that the faults cut the entire volcanic pile to its base, ~8 km below sea level [e.g., Lipman et al., 1985]. Ground deformation and fault displacements associated with the 1975 Kalapana earthquake, however, seem to favor the shallow model for the fault system [e.g., Cannon and Bürgmann, 2001]. Overall displacement of Kīlauea's south flank occurs due to motion on a basal décollement that

lies at the boundary between the volcanic pile and preexisting oceanic crust, coupled with opening of Kīlauea's deep rift zones [Delaney et al., 1990]. The subhorizontal detachment fault is defined by seismicity [e.g., Got and Okubo, 2003; Matoza et al., 2013] and suggested by compressional structures in the submarine portion of the flank [Morgan et al., 2000]. The detachment appears to be actively creeping adjacent to the rift zones and locked offshore [Montgomery-Brown et al., 2015]. Such a kinematic model explains secular flank motion (due to the creeping section), strong earthquakes (due to the locked section), and SSEs (which occur along the transition between the locked and creeping sections). The depth of the décollement has been a source of some debate, since geodetic models are poorly constrained due to the scarcity of offshore deformation data. Joint consideration of seismic and geodetic data, however, favor a depth of ~8 km [Segall et al., 2006] (although the seismic data permit shallower depths as well [Wolfe et al., 2007]), which is also supported by limited submarine vertical displacement data [Phillips et al., 2008]. The position of the fault at the interface between the volcano and ocean crust is consistent with the presence of weak marine sediments at this boundary [Nakamura, 1980; Dieterich, 1988] due to the advanced age of the plate (~95 million years) [Van Ark and Lin, 2004]. Thus, Kīlauea's unstable flank appears to be underlain by a décollement fault at the base of the volcanic pile that transitions from onshore slipping to offshore locked, while at shallower depths the flank hosts normal faults that respond to sudden flank movements.

In contrast to Kīlauea, there is no clear evidence of a décollement plane below the unstable flank of Piton de la Fournaise, although structural discontinuities are suggested by geological and geophysical data. A geological boundary, indicated by a low-seismicity zone and the depth of the upper magma reservoir [e.g. Peltier et al., 2008, 2009; Prôno et al., 2009], appears to be present at sea level [Battaglia et al., 2005], suggesting a neutral buoyancy surface. A few earthquakes have been recorded in the Grandes Pentes area of the east flank, about 2 km below sea level (in 2016, ~10 M<2 events were relocated in this region, although the rest of the volcano's east flank is mostly aseismic), which may be the continuation of a structure marked bya second low-seismicity zone beneath the summit that was observed during migration of earthquakes prior to the 1998 eruption [Battaglia et al., 2005]. According to Gailler et al. [2009], the top of the intrusive layered complex, encountered by a drill hole in the Grand Brûlé area of the lower eastern flank (from about 830 m bsl to 2830 m bsl), could be a glide plane overlain by landslide products, as suggested by Courteaud [1996]. Geologic evidence from Piton des Neiges

and modeling of geodetic data at Piton de la Fournaise guided by those constraints argue that shearing of a magmatic sill that was intruded along a detachment fault could explain the large flank displacements associated with the 2007 distal eruption at the volcano [Chaput et al., 2014], with continued seaward displacements as the co-eruptive motion decays slowly over time. The modeled size of such a sill, however, is not realistic, suggesting that a fault plane is a more viable source of east flank motion [Tridon et al., 2016]. The speculated detachment surface, regardless of its form, is probably not at the interface of the volcanic pile and sea floor, which is 7–8 km beneath the volcano's summit, but might be at the interface between Piton de la Fournaise and the underlying Piton des Neiges, although there are no compressional structures analogous to those on Kīlauea's submarine flank suggesting such a fault plane [Le Friant et al., 2011]. The possibility of a detachment plane beneath the east flank of Piton de la Fournaise therefore remains ambiguous. Another major difference between Piton de la Fournaise and Kīlauea is the lack of surface faulting and relatively simple flank structure on the former.

If Piton de la Fournaise represents the simple end member of flank structure, Etna trends towards the more complex end of the spectrum. Etna's mobile sector is heavily faulted due to the numerous blocks that make up the flank. The most significant flank faults are the NNW-SSE-striking Timpe faults, which usually show normal motion but are also occasionally characterized by reverse displacements [Puglisi et al., 2008]. The latter behavior is associated with an "active pushing" of the mobile flank by dike intrusions [Puglisi et al., 2008] as suggested by 2D analogue experiments [Le Corvec et al., 2014], but has also been observed on the Pernicana fault, which defines the northern boundary of the unstable flank, in association with strong summit inflation [Puglisi et al., 2001; Bonforte et al., 2007a]. Off-shore investigations [Chiocci et al., 2011; Gross et al., 2015] indicate that the continental margin is affected by a wide semicircular fault system that can be interpreted as the expression of a large-scale retrogressive instability extending to a depth of more than 2000 m. Based on these data, we suggest that the on- and off-shore portions of the Timpe fault system are part of the flank instability affecting the continental margin, rather than the northernmost extension of the Malta Escarpment (a major lithospheric fault system separating the thick continental crust of southeastern Sicily to the west from the thin oceanic crust of the Ionian Basin to the east), as has previously been suggested [Ben-Avraham and Grasso, 1991; Hirn et al., 1997]. This interpretation is consistent with GNSS surveys that demonstrate the involvement of the Timpe faults in the eastward motion of the flank

[Bonforte and Puglisi, 2006].

The thickness of the sliding pile on Etna's east flank is not clear. It surely involves the upper part of the sedimentary basement, which outcrops on the mobile part of the northeastern flank up to an altitude of 800 m a.s.l. Conceptual models of the flank suggest a U-shaped sliding sector with a base that may lie between sea level and several kilometers below sea level [Froger et al., 2001; Azzaro et al., 2013, and references therein]. Geophysical data (seismicity, tomography, and resistivity) have not identified a zone of weakness beneath the flank [De Gori et al., 2005; Siniscalchi et al., 2012] but do suggest a change in the pattern of the stress field at ~2-3 km b.s.l. [Alparone et al., 2011]. The depth of a hypothetical detachment level has been inferred only from geological evidence and inversion of ground deformation measured by GNSS. On the middle of the northeastern flank, both geology and geodesy indicate compressional features along the lower half of the Pernicana fault system that may be related to a shallow décollement and/or to rotation of the fault with respect to the motion of the flank [Tibaldi and Groppelli, 2002; Bonforte et al., 2007a]. A deeper sliding plane—at sea level or below—must also exist, given ground deformation measured along the coastline. The depth of such a plane is not easy to model, owing to a lack of seismicity and offshore geodetic data. Two depths have been suggested from inversion of ground deformation data: 1) a deep detachment at 2–3 km b.s.l. that involves a thick portion of the sedimentary basement, suggested also by deformation associated with the 2001 flank eruption [Bonforte and Puglisi, 2006; Bonforte et al., 2009; Ruch et al., 2010; Le Corvec et al., 2014], and 2) a shallower detachment at 0–2 km b.s.l. based on post-eruptive deformation following activity in 2001 and in 2002, when flank motion at sea level accelerated dramatically, models of which require the involvement of the volcanic pile and the uppermost levels of the sedimentary basement [Bonaccorso et al., 2006; Bonforte et al., 2008].

3.3 Interaction with magmatic activity

On all the three volcanoes, seaward motion of the unstable flanks is modulated by magmatic activity. The degree to which magmatic process influence flank instability, however, varies in intensity from being a secondary trigger of ongoing flank motion (at Kīlauea) to being a primary control on the rate of flank slip (at Piton de la Fournaise).

3.3.1 Quiescent periods

"Quiescence" has been largely unknown at Kīlauea since an 18-year period of no eruptions came to an end in 1952. Especially starting with the advent of flank deformation measurements in the 1960s, the volcano has been in a state of constant magmatic activity—if it was not erupting, magma was accumulating beneath the summit [Wright and Klein, 2014]. The closest thing to quiescence might be relatively stable periods of the 1983–present Pu‘u ‘Ō‘ō eruption, when the eruption rate was comparatively constant for months to years at a time and summit deformation was deflationary, indicating that most magma entering the volcano was being transported to the eruption site [Kauahikaua and Miklius, 2003]. During such periods, flank motion was mostly steady, ~8 cm/yr along the coast [Owen et al., 2000a], except during SSEs. Presumably occurring on the décollement at the transition between the creeping and locked portions of the fault, SSEs manifest a periodicity and can be separated into different spatial families [Brooks et al., 2006; Montgomery-Brown et al., 2015]. Since 2003, the events have been larger in magnitude and more periodic in occurrence (2.44 ± 0.15 years) [Montgomery-Brown et al., 2015]. The often-steady motion of the flank and regular occurrence of SSEs, regardless of the magmatic state of the volcano, imply that gravitational spreading is a major driving force of flank deformation. Swanson et al. [1976] speculated that flank motion could be driven by dike intrusion in the shallow rift zone, and such activity undoubtedly does have an impact on short (months to years) timescales, but an alternative mechanism is the flow of dense olivine cumulates beneath the summit and within the deep rift zones [Clague and Denlinger, 1994]. In fact, numerical modeling indicates that gravitational spreading due to flow of dense cumulates can explain long-term secular deformation of Kilauea's south flank [Plattner et al., 2013]. Overprinted on this long-term gravitational spreading are transient magmatic events that are encouraged by persistent flank motion. Dike intrusions in 1997 [Owen et al., 2000b] and 1999 [Cervelli et al., 2002b], for example, were ascribed to a decrease in the least compressive stress across the East Rift Zone owing to seaward flank motion, and SSEs are associated with, and might have triggered, some anomalous magmatic activity [Montgomery-Brown et al., 2015].

Quiescence is more common at Piton de la Fournaise and Etna, where it is manifested as a lack of eruptive activity and summit deflation that can persist for months to years. During the 2010–2014 non-eruptive period at Piton de la Fournaise, seaward motion was relatively steady (Fig. 6), although the behavior of the flank during previous quiescent times is not known owing to a lack of deformation data in this sector before 2010. Summit deflation and seaward-directed

flank motion generates extension within the upper part of the eastern flank [Peltier et al., 2015b]. The situation is much the same at Etna (and Kīlauea), where the east flank moves toward the sea along the coast even when the volcano is not erupting or inflating. Summit deflation combined with flank spreading seems to produce a relaxation of the mobile flank, prompting motion along local faults and causing extension along the NE rift [Bonforte et al., 2008].

3.3.2 Periods of magmatic unrest

At Kīlauea, magmatic activity does not appear to affect the steady long-term seaward motion that has characterized the volcano's southern flank since the start of continuous geodetic observations in the 1990s. For instance, during a surge in magma supply in 2003–2007, when the amount of magma entering the volcano from the mantle more than doubled and inflation occurred at the summit and along the rift zones, there was no significant change in flank displacement rates [Poland et al., 2012, 2014; Anderson and Poland, 2016]. Similarly, no change in the long-term displacement rate of coastal GPS stations was observed following dike emplacement events in the rift zones, like that of 2011 (Fig. 6). Magmatic activity has, however, been observed to trigger short-term transient flank motion in two ways. First, intrusion into, and spreading of, the rift zones, if occurring at a faster rate than flank spreading, can cause compression of the flank [Swanson et al., 1976]. As an example, it is relatively common for M~5 events to occur on the décollement beneath the flank in the days to weeks after rift zone intrusions and dike-fed fissure eruptions [e.g., Poland et al., 2008]. Second, SSEs have been associated with magmatism. The best example is the Father's Day intrusion and eruption of June 2007, when a dike intruded the volcano's East Rift Zone at about the same time that an SSE was expected (based on the occurrence of SSEs in 2003 and 2005). Dike growth, which was initially caused by magma overpressure at the summit, appeared to be waning after ~6 hours of activity when an SSE began, perhaps encouraged by the opening of the initial dike as suggested by stress modeling [Brooks et al., 2008; Montgomery-Brown et al., 2010]. Flank slip facilitated further rift zone opening and the reinvigoration of the intrusion, resulting in the emplacement of a second, larger dike that ultimately reached the surface [Brooks et al., 2008; Poland et al., 2008; Montgomery-Brown et al., 2010, 2015]. This reinvigoration was a consequence of a decrease in the least compressive stress across the rift zone as opposed to magma overpressure. Magmatic activity has also been associated with the occurrence of SSEs in 2005 and 2012; thus, it appears

that SSEs and Kīlauea's magmatic system have the potential to influence one another, but only if either or both of those systems are already close to failure [Montgomery-Brown et al., 2015]. Large flank slip events also have an obvious impact on eruptive and intrusive activity at Kīlauea, as demonstrated by the 1975 earthquake, which created a situation favoring intrusion over eruption for months to years after the earthquake [Dzursin et al., 1980]. Previous episodes of flank slip were associated with similar major changes in eruptive and intrusive behavior [Denlinger and Morgan, 2014].

In stark contrast, flank motion at both Piton de la Fournaise and Etna responds to changes in magmatic activity—specifically, seaward flank motion accelerates during periods of inflation and eruption [e.g., Bonforte et al., 2008; Bonaccorso et al., 2011; Peltier et al., 2015b; Chen et al., in revision]. For example, at Piton de la Fournaise, steady seaward motion accelerated in 2015 across the entire east flank simultaneous with a deep seismic swarm (7 to 1.5 km bsl) 31 days prior to the May 17 eruption, and higher flank motion rates persisted until the onset of the August 24 eruption [Peltier et al., 2016]. Dike emplacement at Piton de la Fournaise is often characterized by an asymmetrical pattern, with seaward motion of the eastern flank and almost no motion of the western flank. This condition has resulted in net displacements of 9.2 ± 2.5 m of displacement to the east and 1.3 ± 2.5 m to the west during 1950–2015 [Derrien et al., 2015]. Distal eruptions are associated with especially significant flank motion, exemplified by the 1.4 m of seaward displacement observed during April 2007 [Froger et al., 2015]. Got et al. [2013] showed that such large plastic motion relaxed the horizontal elastic stress accumulated during the periods between distal eruptions and facilitated lateral transport of magma to eruption sites far from the summit. This strain weakening of the edifice may occur along a plane at depth that favors sill formation, as proposed by Chaput et al. [2014], although Tridon et al. [2016] favor a detachment surface.

At Etna, spreading of the volcano is also clearly enhanced by summit inflation, which promotes accelerated eastward motion of the eastern flank. The inflation is sometimes strong enough to cause the mobile flank to overthrust the stable portion of the volcano, as indicated by the reverse motion of some flank faults [Puglisi et al., 2001; Le Corvec et al., 2014]. This is part of a feedback process [Acocella et al., 2003; Bonaccorso et al., 2011; Alparone et al., 2013], much like that observed in 2007 at Kīlauea, where seaward flank motion encourages magma ascent, and also as has been proposed at Piton de la Fournaise to explain distal eruptions [Got et

al., 2013]. The feedback can be strong enough that some lateral eruptions are considered to be favored or triggered by the flank motion, with stored magma erupting from extensional fractures caused by stretching induced by the spreading [Bonaccorso et al., 2006]. Forceful dike intrusion can also provide a "push" to the flank. In the long-term, both "active" (i.e., triggered by magma overpressure) and "passive" (i.e., triggered by rift opening) processes have been observed as part of a continuous feedback between flank motion and magma dynamics [Alparone et al., 2013; Acocella et al., 2016]. Lateral and eccentric dike intrusions strongly modify the local stress pattern at Etna and, consequently, modulate spreading of the mobile sector of the volcano. In 2001, for example, the intrusion of an eccentric dike on the upper south flank of the volcano was part of a positive feedback with instability of the eastern flank [Billi et al., 2003; Bonforte et al., 2009]. Deformation data indicate that a flank fault that slipped in one direction during the intrusion reversed its direction of slip during the subsequent eruption, and after a few weeks an increase in lower flank seismicity and seaward motion occurred [Puglisi et al., 2008]. In contrast to 2001, the 2002 intrusion on the NE rift was at least partially promoted by flank motion that caused extension across the rift, especially its upper part, as indicated by deformation and gravity data [Bonforte et al., 2007b; Ruch et al., 2012]. The reaction of the mobile flank to the 2002 intrusion included large and immediate displacements along the Pernicana fault [Bonforte et al., 2007a; Alparone et al., 2013] and, after a few days, also of other faults that dissect the sliding flank [Acocella et al., 2003]. The intrusion of the dike that fed the 2008-09 eruption was partially controlled by flank dynamics [Bonforte et al., 2013c], while, in turn, a very shallow dike intrusion in 2014 seems to have come close to triggering a slope failure on the upper part of Valle del Bove [Bonforte and Guglielmino, 2015].

4. Conceptual framework for persistent flank instability

The above review of flank characteristics at Kīlauea, Piton de la Fournaise and Etna highlights the strong relation that exists between the factors controlling long-term persistent flank instability (gravitational spreading and magmatic forces, as well as structural setting) and its expression at surface. These three volcanoes define a broad spectrum in terms of these factors (Table 1), and this range is responsible for the observed differences in the manifestations of ongoing flank deformation.

4.1 The spectrum of persistent, long-term instability

Even though the overall deformation style on the three volcanoes we reviewed is similar—persistent seaward displacement of the unbuttressed flank in the direction perpendicular to the bounding rift zones—the characteristics of the deformation are quite different. Flank faulting varies widely, with Etna displaying independently moving blocks, Kīlauea with fault systems that respond to large earthquakes but possibly not to steady creep, and no visible major faulting on the mobile flank of Piton de la Fournaise. The displacement rates vary as well, being much higher at Kīlauea (Fig. 6), which has the highest magma supply and is the largest edifice of the three (Table 1). The surfaces that accommodate the motion may also be very different. At Kīlauea, flank slip occurs along the boundary between the preexisting ocean floor and the volcanic pile, lubricated by the presence of weak oceanic sediments. The sliding surfaces at Piton de la Fournaise and Etna are much less well known owing to a lack of geophysical evidence that strongly delineates the presence of a plane of weakness. While the depths vary significantly (8–10 km beneath the surface at Kīlauea to possibly less than a few km at Piton de la Fournaise and Etna), in all three cases the slip plane is probably associated with a weak boundary layer, be it sediment, a sill, or some other geological discontinuity. Weak sedimentary layers or geological boundaries have long been highlighted as necessary factors in accommodating volcanic spreading [e.g., Borgia et al., 1992, 2000], and appear critical for supporting long-term persistent instability at large basaltic edifices.

The varying role of magma pressure versus gravitational spreading in flank processes appears to correlate with the size of the volcano. Kīlauea experiences steady flank motion that can be explained as primarily due to gravitational spreading [Clague and Denlinger, 1994; Plattner et al., 2013], perhaps because the volcano is the largest of the three we examined (Table 1) and has a dense core. Magmatic activity is a secondary factor that influences flank processes only when the décollement is already close to failure (e.g., when an SSE is about to occur anyway [Montgomery-Brown et al., 2015]) or when the flank is temporarily put into a state of compression by shallow intrusions [Swanson et al., 1976]. Similarly, flank slip impacts the magmatic system when magma is already primed for eruption or intrusion, as with the buildup of rift zone extension prior to the 1997 and 1999 dike intrusions [Owen et al., 2000b; Cervelli et al., 2002b], or during the 2007 intrusion-SSE-intrusion sequence [Montgomery-Brown et al., 2010, 2015]. Flank instability at both Piton de la Fournaise and Etna, in contrast, is characterized by a

much stronger response to changing magmatic conditions, with episodes of flank motion being triggered by, and further triggering, eruptive and intrusive activity. At all three volcanoes, rift zones play an important role by defining the boundary of the unstable flank, with little motion on the "stable" side. Rift zone development is strongly tied to instability [e.g., Walter et al., 2005], given the strong positive feedback between rift opening and flank displacements [e.g., Poland, 2014a] due to the buildup of steep, unstable slopes, especially in triple-armed rifts [Carracedo, 1999], or from volcanic spreading [Münn et al., 2006].

Although catastrophic collapse is widespread among large volcanic edifices, persistent, long-term instability has been identified on only a few volcanoes worldwide. In addition to Kīlauea, Piton de la Fournaise, and Etna, Mauna Loa has a steadily moving flank. The rate of motion (a few cm/yr) is intermediate between Kīlauea and Etna but is occurring on the flank that abuts Kīlauea [Miklius et al., 1995]—a testament to the size of Mauna Loa and the gravitational force driving the instability (apparently, even buttressed flanks can creep given enough force, although Kīlauea is growing on the flank of Mauna Loa, and its volume is a small fraction of Mauna Loa's [Lipman and Calvert, 2013]). Flank creep of a few mm/yr has also been documented using a large InSAR dataset at Cumbre Vieja volcano, La Palma, Canary Islands, where the deformation may be due to sliding along buried sediments or debris avalanche deposits [González et al., 2010]. Structural studies have suggested flank creep at other volcanoes as well, like Mt. Cameroon, West Africa [Mathieu et al., 2011], although no geodetic results have confirmed this possibility (it may be that such deformation is below detection thresholds, except, perhaps, when the volcano enters a period of magmatic unrest). Flank creep was suspected at Fogo, Cape Verde Islands, on the basis of structural studies of the 1951 and 1995 eruptions [Day et al., 1999], but there was no evidence from geodetic studies of the 1995 [Amelung and Day, 2002] or 2014–2015 [González et al., 2015] eruptions to corroborate this hypothesis. Fogo, however, is characterized by a collapse scar on its east flank—indeed, many ocean island volcanoes without persistent motion show evidence of catastrophic collapse, like Tristan da Cunha and El Hierro [Holcomb and Searle, 1991]. The Sciara del Fuoco scar on the northwest flank of Stromboli volcano is a result of a huge sector collapse [Tibaldi, 2001], and there is downslope motion of that flank that is modulated by eruptive activity [Di Traglia et al., 2014], but the motion appears to be related to the stability of lava flows on this steep slope [Bonaccorso et al., 2009; Bonforte et al. 2016]. Past collapses on these volcanoes may have been associated

with persistent flank motion prior to failure, although this remains speculative without supporting models or observations. At all volcanoes where persistent flank motion has been documented or hypothesized, the moving flank is along the coast (even at non-ocean-island volcanoes, like Etna) and largely unbuttressed by significant topography. While such a condition may not be sufficient to cause persistent flank motion, it may be necessary to sustain long-term instability [e.g., Froger et al., 2001; Norini and Acocella, 2011].

4.2 Factors controlling persistent flank instability

From our comparative analysis, the occurrence of long-term continuous flank instability at large basaltic volcanoes seems to require at least two conditions: (1) the presence of a weak, subhorizontal layer within the subsurface upon which sliding can occur, and (2) gravitational spreading and/or magmatic force to cause internal edifice strain weakening and motion along the weak layer (such force may be counteracted by the buttressing presence of an adjacent volcano or other topography, explaining why persistent instability has thus far only been observed in island and coastal environments). This conclusion is not new. Many other authors have recognized the combination of gravitational/magmatic loading and weak basement on volcanic spreading [e.g., van Wyk de Vries and Borgia, 1996; Borgia et al., 2000]. The combination of these factors, however, must be relatively rare when it comes to large basaltic edifices, given the global paucity of persistent flank instability on such volcanoes. It may therefore be helpful to define a framework for long-term flank instability of large basaltic volcanoes based on these factors as a means of understanding why a particular volcano may or may not be characterized by persistent flank motion.

Subhorizontal planes of weakness can have numerous forms, and their presence seems to depend largely upon the setting in which a volcano grows. Sediment on old oceanic plates provides a lubricating layer upon which sliding could occur, as is the case in Hawai‘i, where the Pacific Plate is about 95 million years old. Although Piton de la Fournaise is also located on an old oceanic plate (~66 million years old), it is growing on the flank of the preexisting Piton des Neiges volcano. The interface between the two edifices provides a boundary layer upon which flank sliding may occur in this case, although it is also possible that a sill intrusion or layered intrusive complex is the weak layer. Unlike the other two volcanoes, Etna lies at a convergent margin, where sedimentary basement rocks are a likely source of weakness beneath the sliding

east flank. Volcanoes that do not have thick weak layers beneath them seem to be less prone to long-term persistent flank instability (although not necessarily less prone to catastrophic collapse). For instance, the volcanoes of the western Galápagos have grown simultaneously upon ~10-million-year-old ocean floor with little sedimentary cover, so there is no obvious weak layer beneath any of the volcanoes (in addition, the volcanoes buttress one another, except on the western sides of the western-most volcanoes) [Nakamura, 1980; Chadwick and Dieterich, 1995; Poland, 2014a]. In this light, the lack of creep on volcanic flanks in the Galápagos is not surprising.

When a weak layer is present, the force needed to drive persistent flank instability can be provided by gravitational spreading and/or magmatism. To be dominated by gravitational spreading requires that a volcano be massive, which in turn implies a very high rate of magma supply to the edifice and/or a slow rate of plate motion (which governs the amount of time that a volcano is connected to its magma source in the case of hotpot volcanoes). Hawai‘i is the only case of the three studied here where, thanks to the great rate of melt production, volcanoes can grow in size to tens of thousands of km^3 despite the relatively fast motion of the Pacific Plate (Table 1), which limits vigorous volcanism at a given volcano to few hundred thousand years [Lipman and Calvert, 2013; Clague and Sherrod, 2014]. The importance of melt production is evident in comparing Kīlauea and Piton de la Fournaise—Kīlauea is an order of magnitude larger in volume, owing to its higher magma supply rate, yet Piton de la Fournaise is longer lived, since it sits on a much more slowly moving plate (Table 1) [Peltier et al., 2015a]. The rapid flank motion at Kīlauea may therefore be a natural consequence of, and provide a balance for, the high and continuous magma supply to the volcano, which constructs a massive edifice. At smaller volcanoes, like Etna and Piton de la Fournaise, magmatic forces play a larger role in the occurrence of long-term flank instability, as demonstrated by the correlation between changes in flank motion rate and intrusive/eruptive activity. In fact, flank instability at Piton de la Fournaise and Etna may be a geologically recent phenomenon. The contemporary magma supply to both volcanoes is an order of magnitude higher than their overall growth rates (edifice volume divided by volcano age; Table 1), so current high rates of magma supply to both volcanoes (relative to their overall growth rates) might drive observed flank motion. Regardless, a common factor among all three volcanoes is high, and quasi-continuous, magma supply, which therefore seems a strong factor in developing and sustaining long-term persistent instability.

An examination of the relationships between maximum flank displacement rate, edifice size, and magma supply supports the inference that volcanoes with high rates of magma supply are most prone to develop persistent flank instability, with edifice size also playing a role (especially in the case of gravitational spreading versus magma-driven flank motion; Fig. 7). Cumbre Vieja does manifest flank instability despite its low magma supply rate (probably similar to that of nearby El Hierro—about 0.002 km^3/yr [González et al., 2013]—based on comparable recent eruptive history) and has a volume of several thousand km^3 [Schmincke, 1982], and the flank may be underlain by debris avalanche or sedimentary deposits [González et al., 2010]. The lack of magmatic activity coincident with the observed flank deformation suggests that a weak layer plus the volcano's size may be sufficient to drive a small amount of persistent flank motion (volcanoes with similar sizes and magma supply rates, like El Hierro and Fogo, have experienced catastrophic collapses, possibly removing flanks that were subject to persistent motion). Conversely, some Galápagos volcanoes have comparatively high rates of magma supply but no persistent flank motion, emphasizing the importance of a weak substrate for sustaining instability.

4.3 Long-term persistent flank instability: a conceptual framework

Given the relationships between magma supply, edifice size, and volcanic basement, a useful framework for understanding long-term persistent flank instability may be the interplay between the structural setting of a volcano, which governs the presence and thickness of any underlying weak layer, and the magmatic activity of the volcano, which controls edifice size and magma supply [Borgia et al., 2000]. Volcanoes underlain by thick, weak layers and that have high magma supply rates or that are very large are more prone to the development of persistent flank instability compared to volcanoes lacking one or more of these elements. Plotting volcanoes in the two-dimensional space defined by magmatic activity and structural setting demonstrates that a distinction can be drawn between volcanoes with persistent flank instability and those without (Fig. 8). Such a plot is inherently schematic in nature, owing to the fact that edifice size and magma supply are somewhat independent (for instance, El Hierro is larger in volume than Piton de la Fournaise, yet has a lower magma supply), but is nonetheless illustrative of overall patterns in the characteristics of persistent flank motion. Hawai‘i defines an extreme in this spectrum—old, sediment-covered substrate and large edifices fed by high magma supply—

so it is not surprising that flank instability is so intense there. The high rates of flank deformation in Hawai‘i are driven in large part by gravitational spreading (with secondary magmatic forcing) due to the extreme size of the edifices and dense cumulates at the cores of the volcanoes [Clague and Denlinger, 1994; Brooks et al., 2008; Montgomery-Brown et al., 2010, 2015; Plattner et al., 2013]. Piton de la Fournaise and Etna also sit on weak layers of some sort and have relatively high magma supply, but not to the extreme of Kīlauea and Mauna Loa, so the volcanoes are smaller, and flank slip occurs at a lower rate and is influenced to a greater extent by magmatism. Cumbre Vieja instability must be driven by gravitational spreading, given the lack of recent magmatic activity (its most recent eruption was in 1971 [González et al., 2010]) and its relatively large volume. The rate of flank motion (a few mm/yr) is smaller than that recorded at Etna and Piton de la Fournaise (a few cm/yr); however, flank motion rates might change drastically during an episode of magmatic unrest, by analogy with Piton de la Fournaise and Etna. Even though some Galápagos volcanoes, like Sierra Negra, have magma supply rates comparable to that of Piton de la Fournaise (Fig. 7) [Poland, 2014a], the volcanoes are relatively small and sitting on young ocean floor with little sedimentary cover, and therefore not prone to persistent flank motion (Fig. 8).

Since Cumbre Vieja shows signs of persistent instability, shouldn’t other volcanoes in the Canary Islands, which have similar geologic settings, sizes, and magmatic activity, also be characterized by creeping flanks? It is possible that such deformation is occurring but has yet to be detected because it is so small. Indeed, Tenerife is subsiding by a few mm/yr, likely due to gravitational loading of weak lithosphere [Fernández et al., 2009]. La Palma and El Hierro, being the most westward of the Canary Islands, are unbuttressed to the west and, therefore, are a logical place to look for flank motion. El Hierro has experienced multiple catastrophic collapses [Holcomb and Searle, 1991; Masson et al., 2002], so its subaerial flanks are small and may not be deforming at this time (although one might speculate that they were moving persistently prior to their collapse, which might also have been the case at Fogo—a volcano of similar volume and eruptive activity and also sitting on old ocean floor). It is also possible that low and discontinuous magma supply to volcanoes like Fogo and El Hierro may obscure manifestation of persistent creep-like instability. Volcanoes exemplified by Cumbre Vieja, El Hierro, and Fogo therefore appear to lie at the boundary between the presence and absence of persistent flank motion; flank creep may occur, but at very low deformation rates that are difficult to detect. An

806 additional instance of this scenario, albeit located on younger seafloor, is provided by Pico,
807 Azores. An active slump on the southeast side of the Pico volcanic ridge is suggested by flank
808 deformation and morphology; seaward horizontal displacements are at about the level of
809 detection, but subsidence may reach rates of ~1 cm/yr [Hildenbrand et al., 2012].
810 The framework of magmatic activity versus structural setting may also explain the style
811 of flank faulting. High magma supply, a large edifice volume, and a subvolcanic weak layer can
812 result in a heavily faulted flank, as is the case at Etna, Kīlauea, and Mauna Loa. Piton de la
813 Fournaise has comparatively lower magma supply, is smaller in volume, and may have a less-
814 developed weak layer, and so the flank has not been heavily faulted. Cumbre Vieja is a relatively
815 large edifice and is underlain by thick oceanic sediments (based on the age of the sea floor), but a
816 lack of strong magmatic activity may not be conducive to flank faulting.
817
818 **5. Conclusions**
819 Although Kīlauea, Piton de la Fournaise, and Etna are each characterized by persistent
820 flank motion, the manifestations and mechanisms of the process at the three volcanoes cover a
821 wide range. At Kīlauea, persistent instability is driven mostly by gravitational spreading of
822 magmatic cumulates and accommodated along a detachment fault at 8–10 km depth, and the
823 flank is heavily faulted (although the faults may only rupture during strong earthquakes). At Etna
824 and Piton de la Fournaise, flank motion is driven to a greater extent by magmatism, and the plane
825 along which motion occurs is poorly known but probably within a few km of the surface. Etna's
826 flank is heavily faulted with blocks that move independently, while the flank of Piton de la
827 Fournaise shows no obvious signs of faulting.
828 The similarities and differences in flank motion at the three volcanoes can be expressed
829 in terms of structural setting and magmatic activity. Volcanoes that grow to great size,
830 presumably due to high rates of magma supply and/or long durations of activity, can develop
831 instabilities that are governed by gravitational spreading. Flank motion at smaller volcanoes but
832 that have frequent eruptions and intrusions may be more highly influenced by magmatism, which
833 may in turn be related to the extent of flank faulting (higher at Etna, which is supplied by a
834 greater rate of magma supply compared to Piton de la Fournaise). In all cases, a subhorizontal
835 plane of weakness of some sort is a necessary component for persistent flank instability;
836 volcanoes lacking such a weak layer, like those of the Galápagos, show no signs of long-term

flank motion (though catastrophic flank collapse may still occur). An unbuttressed flank may also be a requirement for accommodating flank slip, although such a condition is not strictly required (as demonstrated by Mauna Loa), nor is it a specific trigger for persistent instability.

We suggest that the framework of magmatic activity versus structural setting may be a useful starting point for understanding the spectrum of potential long-term persistent flank instability at large basaltic volcanoes around the world—why sliding flanks are common in some places but absent in others, and how sliding flanks vary from volcano to volcano. Such a framework provides a convenient, if subjective, means of understanding this complex process, evaluating its importance, and interpreting its surface expression at volcanoes that may be less well understood than our three example edifices. Further, the proposed conceptual model is a good alternative to the use of any one specific volcano as an analog. Kīlauea is often cited as a "type example" for flank instability, thanks to the long history of study and, by association, more developed understanding of the process, but the example is an extreme one that does not necessarily translate well to other volcanoes (except, perhaps, Mauna Loa, which is similar in size, setting, and magmatic activity).

We also hope that our proposed framework can serve as a starting point for investigating volcanoes that experience catastrophic collapse. Although they are infrequent, large landslides represent a potentially devastating hazard, and the conditions of their occurrence are poorly understood. Perhaps the most poignant question is whether or not flanks characterized by persistent long-term motion will eventually collapse catastrophically. By connecting future models of flank collapse with the framework we have proposed here, it may be possible to develop a better overall understanding of all forms of flank instability.

Acknowledgments

Funding for this work was provided by the U.S. Geological Survey, by Agence Nationale de la Recherche under contract ANR-16-CE04-0004-01 (SlideVOLC), and by the European MEDSUV project. We are grateful for helpful comments from Dan Dzurisin, and thorough reviews by Ingrid Johanson, Bill Chadwick, and Valerio Acocella. This is IPGP contribution n°3837.

Figure Captions

Figure 1. Map showing locations of large basaltic volcanoes discussed in the text.

Figure 2. Shaded relief map of Kīlauea Volcano, Hawaii, showing major structural features discussed in the text.

Figure 3. Shaded relief map of Piton de la Fournaise volcano, La Réunion, showing major structural features discussed in the text.

Figure 4. Shaded relief map of Etna volcano, Sicily, showing major structural features discussed in the text. TL: Tindari-Letojanni fault; ME: Malta Escarpment; CG: Catania-Gela foredeep.

Figure 5. Flank displacements determined from GNSS at (A) Kīlauea, (B) Piton de la Fournaise, and (C) Etna. Time periods shown correspond to periods of steady eruptive activity and summit subsidence at Kīlauea (1997–2002), of magmatic quiescence at Piton de la Fournaise (2012–2013) and of summit eruptions at Etna (2012–2016).

Figure 6. Time series of flank displacement at Kīlauea (red), Etna (blue), and Piton de la Fournaise (black) at the GNSS station located closest to the coastlines at each volcano. The three offsets in the Kīlauea time series are the results of an East Rift Zone fissure eruption in 2011 and slow slip events (SSEs) in 2012 and 2015.

Figure 7. Plots showing relations between magma supply (top) and edifice size (bottom) versus the maximum rate of horizontal flank motion. Values are from Table 1, Schmincke [1982], González et al. [2010; 2013], Poland [2014a], and Bagnardi et al. [2016]. Volcanoes of the Canary and Galápagos archipelagos are grouped, given their internal similarities in size and magma supply. Red labels indicate volcanoes with persistent flank motion (in the case of the Canary Islands, only Cumbre Vieja is known to have a persistently moving flank).

Figure 8. Conceptual framework for understanding persistent long-term flank instability. X-axis defines magma supply and/or edifice size (noting that a large edifice is possible under conditions of low magma supply if plate velocity is low) increasing to the right, and Y-axis is structural setting, increasing in thickness of weak substrate upward. Rates of flank motion increase with magmatic activity and structural setting, with gravitational spreading being the dominant driving mechanism at larger volcanoes, and flank faulting important where magma supply is highest.

Table 1. Comparison of the general characteristics of Kīlauea, Piton de la Fournaise, and Etna volcanoes. Numbers in brackets give references for specific characteristics.

Characteristic	Kīlauea	Piton de la Fournaise	Etna
Volume	31,600–11,000 km^3 [1,2]	~1500 km^3 [3]	~684 km^3 [4]
Plate tectonic setting	Intraplate; 10 cm/yr plate velocity [5]	Intraplate; 2 cm/yr plate velocity [5]	Plate boundary (convergent)
Age	~275 ka (inception), ~100 ka (shield) [1]	~500 ka [6]	~500 ka (tholeiitic), ~200 ka (basaltic) [7]
Magma supply	~0.1 km^3/yr [8]	0.01–0.04 km^3/yr [9,10]	~0.075 km^3/yr [11]
Detachment	Yes, between volcanic pile and ocean floor; many earthquakes	No clear evidence, possible sill or along interface with Piton des Neiges; some earthquakes 1-2 km b.s.l.	No clear evidence, possible in the sedimentary basement; no earthquakes along possible detachment
Flank faulting	Normal faults parallel to coast; no clear evidence of motion except during large earthquakes	No apparent flank faulting	Normal and strike-slip faults, azimuths linked to regional tectonic setting and dynamics to volcanic activity
Horizontal displ. from flank instability	Velocity increases to the coast; max ~8 cm/yr [12]	Velocity is similar at different elevations during rest periods; ~1.4 cm/yr [13]	Velocity increases to the coast; max 3–5 cm/yr [14,15]
Vertical displ. from flank instability	Uplift along the coast	Subsidence, mostly due to compaction of recent lava flows	Subsidence along the coast (eastward of the Timpe faults)
Interaction with summit magmatism	Not obvious	Increased flank motion during summit inflation	Increased flank motion during summit inflation
Interaction with flank/rift magmatism	Intrusions encouraged by flank motion; slow slip events promote and are promoted by rift zone eruptions and intrusions	Strong flank motion associated with distal eruptions; relaxation time of months–years	Strong flank motion due to rift zone intrusions and eruptions; relaxation time of months–years

[1] Lipman and Calvert, 2013
[2] Robinson and Eakins, 2006
[3] Villeneuve et al., 2014
[4] Bisson et al., 2016
[5] Gripp and Gordon, 2002
[6] Gillot and Nativel, 1989
[7] Branca et al., 2011
[8] Poland et al., 2014
[9] White, 1993
[10] Peltier et al., 2009
[11] Allard et al., 2006
[12] Owen et al., 2000a
[13] Peltier et al., 2015b
[14] Solaro et al., 2010
[15] Bonforte et al., 2011

References

Acocella, V., Behncke, B., Neri, M. and D'Amico, S., 2003. Link between major flank slip and 2002–2003 eruption at Mt. Etna (Italy). Geophys. Res. Lett., 30(24): doi:10.1029/2003GL018642.

Acocella, V., Neri, M., Behncke, B., Bonforte, A., Del Negro, C., Ganci, G., 2016. Why Does a Mature Volcano Need New Vents? The Case of the New Southeast Crater at Etna. Front. Earth Sci., 4: 67, doi:10.3389/feart.2016.00067.

Allard, P., Behncke, B., D'Amico, S., Neri, M., Gambino, S., 2006. Mount Etna 1993–2005: Anatomy of an evolving eruptive cycle. Earth Sci. Rev., 78(1–2): 84–114, doi:10.1016/j.earscirev.2006.04.002.

Alparone, S., Barberi, G., Bonforte, A., Maiolino, V., Ursino, U., 2011. Evidence of multiple strain fields beneath the eastern flank of Mt. Etna volcano (Sicily, Italy) deduced from seismic and geodetic data during 2003–2004. Bull. Volcanol., 73(7): 869–885, doi:10.1007/s00445-011-0456-1.

Alparone, S., Bonaccorso, A., Bonforte, A., Currenti, G., 2013. Long-term stress-strain analysis of volcano flank instability: The eastern sector of Etna from 1980 to 2012. J. Geophys. Res., 118(9): doi:10.1002/jgrb.50364.

Amelung, F. and Day, S., 2002. InSAR observations of the 1995 Fogo, Cape Verde, eruption: Implications for the effects of collapse events upon island volcanoes. Geophys. Res. Lett., 29(12): doi:10.129/2001GL013760.

Anderson, K.R., and Poland, M.P., 2016. Bayesian estimation of magma supply, storage, and eruption rates using a multiphysical volcano model: Kīlauea Volcano, 2000–2012. Earth Planet. Sci. Lett., 447: 161–171, doi:10.1016/j.epsl.2016.04.029.

Azzaro, R., 2004. Seismicity and active tectonic in the Etna region: constrain for seismotectonic model. In: Bonaccorso A., Calvari S., Coltelli M., Del Negro C., Falsaperla S. (Eds.), Mt. Etna Volcano Laboratory. Am. Geoph. Union Geophys. Mono., 143, pp. 205–220, doi:10.1029/143GM13.

Azzaro, R., Bonforte, A., Branca, S., Guglielmino, F., 2013. Geometry and kinematics of the fault systems controlling the unstable flank of Etna volcano (Sicily). J. Volcanol. Geotherm. Res. 251: 5–15, doi:10.1016/j.jvolgeores.2012.10.001.

Bachèlery, P., 1981. Le Piton de la Fournaise (Ile de La Réunion). Etude volcanologique, structural et pétrologique. PhD Thesis, Univ. Clermont-Ferrand II, 215 p.

Bagnardi, M., González, P.J. and Hooper, A., 2016. High-resolution digital elevation model from tri-stereo Pleiades-1 satellite imagery for lava flow volume estimates at Fogo Volcano. Geophys. Res. Lett., 43(12): 6267–6275, doi:10.1002/2016GL069457.

Barreca, G., Bonforte, A., Neri, M., 2013. A pilot GIS database of active faults of Mt. Etna (Sicily): A tool for integrated hazard evaluation. J. Volcanol. Geotherm. Res. 251: 170–186, doi:10.1016/j.jvolgeores.2012.08.013.

Battaglia, J., Ferrazzini, V., Staudacher, T., Aki, K., Cheminée, J.L., 2005. Pre-eruptive migration of earthquakes at the Piton de La Fournaise volcano (Réunion Island). Geophys. J. Int. 161(2): 549–558, doi:10.1111/j.1365-246X.2005.02606.x.

Ben-Avraham, Z., Grasso, M., 1991. Crustal structure variations and transcurrent faulting at the eastern and western margins of the eastern Mediterranean. Tectonophys., 75(3–4): 269–277, doi:10.1016/0040-1951(91)90326-N.

Billi, A., Acocella, V., Funiciello, R., Giordano, G., Lanzafame, G. and Neri, M., 2003. Mechanisms for ground-surface fracturing and incipient slope failure associated with the

2001 eruption of Mt. Etna, Italy: Analysis of ephemeral field data. J. Volcanol. Geotherm. Res., 122(3): 281–294, doi:10.1016/S0377-0273(02)00507-3.

Bisson, M., Spinetti, C., Neri, M. and Bonforte, A., 2016. Mt. Etna volcano high-resolution topography: Airborne LiDAR modelling validated by GPS data. Int. J. Digital Earth, 9(7): 710–732, doi:10.1080/17538947.2015.1119208.

Bonaccorso, A., Bonforte, A., Guglielmino, F., Palano, M., Puglisi G., 2006. Composite ground deformation pattern forerunning the 2004-2005 Mount Etna eruption. J. Geophys. Res., 111(B12): doi:10.1029/2005jb004206.

Bonaccorso, A., Bonforte, A., Gambino, S., Mattia, M., Guglielmino, F., Puglisi, G., Boschi, E., 2009. Insight on recent Stromboli eruption inferred from terrestrial and satellite ground deformation measurements. J. Volcanol. Geotherm. Res., 182(3–4): 172–181, doi:10.1016/j.jvolgeores.2009.01.007.

Bonaccorso, A., Bonforte, A., Currenti, G., Del Negro, C., Di Stefano, A., Greco, F., 2011. Magma storage, eruptive activity and flank instability: Inferences from ground deformation and gravity changes during the 1993–2000 recharging of Mt. Etna volcano. J. Volcanol. Geotherm. Res., 200(3–4): 245–254, doi:10.1016/j.jvolgeores.2011.01.001.

Bonali, F., Corazzato, C., Tibaldi, A., 2011. Identifying rift zones on volcanoes: An example from La Réunion Island, Indian Ocean. Bull. Volcanol. 73(3): 347–366, doi:10.1007/s00445-010-0416-1.

Bonforte, A., Puglisi, G., 2003. Magma uprising and flank dynamics on Mount Etna volcano, studied using GPS data (1994–1995). J. Geophys. Res., 108(B3), 2153: doi:10.1029/2002JB001845.

Bonforte, A., Puglisi, G., 2006. Dynamics of the eastern flank of Mt. Etna volcano (Italy) investigated by a dense GPS network. J. Volcanol. Geotherm. Res., 153(3–4): 357–369, doi:10.1016/j.jvolgeores.2005.12.005.

Bonforte, A., Guglielmino, F., 2015. Very shallow dyke intrusion and potential slope failure imaged by ground deformation: The 28 December 2014 eruption on Mount Etna. Geophys. Res. Lett., 42(8): 2727–2733, doi:10.1002/2015GL063462.

Bonforte, A., Branca, S., Palano, M., 2007a. Geometric and kinematic variations along the active Pernicana fault: Implication for the dynamics of Mount Etna NE flank (Italy). J. Volcanol. Geotherm. Res., 160(1–2): 210–222, doi:10.1016/j.jvolgeores.2006.08.009.

Bonforte, A., Carbone, D., Greco, F., Palano, M., 2007b. Intrusive mechanism of the 2002 NE-rift eruption at Mt Etna (Italy) modelled using GPS and gravity data. Geophys. J. Int., 169(1): 339–347, doi:10.1111/j.1365-246X.2006.03249.x.

Bonforte A., Bonaccorso, A., Guglielmino, F., Palano, M., Puglisi, G., 2008. Feeding system and magma storage beneath Mt. Etna as revealed by recent infation/deflation cycles. J. Geophys. Res. 113(5): doi:10.1029/2007JB005334.

Bonforte, A., Gambino, S., Neri, M., 2009. Intrusion of eccentric dikes: The case of the 2001 eruption and its role in the dynamics of Mt. Etna volcano. Tectonophys., 471(1–2): 78–86, doi:10.1016/j.tecto.2008.09.028.

Bonforte, A., Guglielmino, F., Coltelli, M., Ferretti, A., Puglisi, G., 2011. Structural assessment of Mount Etna volcano from Permanent Scatterers analysis, Geochem. Geophys. Geosyst., 12(2): doi:10.1029/2010GC003213.

Bonforte, A., Carnazzo, A., Gambino, S., Obrizzo, F., Puglisi, G., 2013a. A multidisciplinary study of an active fault crossing urban areas: The Trecastagni Fault at Mt. Etna (Italy). J. Volcanol. Geotherm. Res., 251: 41–49, doi:10.1016/j.jvolgeores.2012.05.001.

1011 Bonforte, A., Federico, C., Giammanco, S., Guglielmino, F., Liuzzo, M., Neri, M., 2013b. Soil
1012 gases and SAR measurements reveal hidden faults on the sliding flank of Mt. Etna (Italy).
1013 J. Volcanol. Geotherm. Res., 251: 27–40, doi:10.1016/j.jvolgeores.2012.08.010.
1014 Bonforte, A., Guglielmino, F., Puglisi, G., 2013c. Interaction between magma intrusion and flank
1015 dynamics at Mt. Etna in 2008, imaged by integrated dense GPS and DInSAR data.
1016 Geochem. Geopys. Geosyst., 14(8): 2818–2835, doi:10.1002/ggge.20190.
1017 Bonforte, A., Gonzalez, P.J., Fernandez, J., 2016. Joint Terrestrial and Aerial Measurements to
1018 Study Ground Deformation: Application to the Sciara Del Fuoco at the Stromboli Volcano
1019 (Sicily). Rem. Sens., 8(6): 463, doi:10.3390/rs8060463.
1020 Borgia, A., Ferrari, L. and Pasquarè, G., 1992. Importance of gravitational spreading in the
1021 tectonic and volcanic evolution of Mount Etna. Nature, 357(6375): 231–235,
1022 doi:10.1038/357231a0.
1023 Borgia, A., Delaney, P.T. and Denlinger, R.P., 2000. Spreading Volcanoes. Ann. Rev. Earth
1024 Planet. Sci., 28: 539–570, doi:10.1146/annurev.earth.28.1.539.
1025 Branca, S., Del Carlo, P., 2004. Eruptions of Mt. Etna during the past 3,200 years: A revised
1026 compilation integrating the historical and stratigraphic records. In: Bonaccorso A., Calvari
1027 S., Coltelli M., Del Negro C., Falsaperla S. (Eds.), Mt. Etna Volcano Laboratory. Am.
1028 Geoph. Union Geophys. Mono., 143, pp. 1–27, doi:10.1029/143GM02.
1029 Branca, S., Coltelli, M., Groppelli, G., Lentini, F., 2011. Geological map of Etna volcano,
1030 1:50,000 scale. Ital. J. Geosci. 130(3): 265–291, doi:10.3301/IJG.2011.15.
1031 Brenguier, F., Kowalski, P., Staudacher, T., Ferrazzini, V., Lauret, F., Boissier, P., Catherine, P.,
1032 Lemarchand, A., Pequegnat, C., Meric, O., Pardo, C., Peltier, A., Tait, T., Shapiro, N.M.,
1033 Campillo, M., Di Muro, A., 2012. First results from the UnderVolc high resolution seismic
1034 and GPS network deployed on Piton de la Fournaise volcano. Seismol. Res. Lett. 83(7):
1035 97–102, doi:10.1785/gssrl.83.1.97.
1036 Brooks, B.A., Foster, J.H., Bevis, M., Frazer, L.N., Wolfe, C.J. and Behn, M., 2006. Periodic
1037 slow earthquakes on the flank of Kilauea volcano, Hawaii. Earth Planet. Sci. Lett., 246(3–4):
1038 207–216, doi:10.1016/j.epsl.2006.03.035.
1039 Brooks, B.A., Foster, J., Sandwell, D., Wolfe, C.J., Okubo, P., Poland, M. and Myer, D., 2008.
1040 Magmatically triggered slow slip at Kilauea Volcano, Hawaii. Science, 321(5893): 1177,
1041 doi:10.1126/science.1159007.
1042 Calvari, S., Tanner, L.H., Groppelli, G., Norini, G., 2004. Valle del Bove, Eastern Flank of Etna
1043 volcano: A comprehensive model for the opening of the depression and implications for
1044 future hazards. In: Bonaccorso A., Calvari S., Coltelli M., Del Negro C., Falsaperla S.
1045 (Eds.), Mt. Etna Volcano Laboratory. Am. Geoph. Union Geophys. Mono., 143, pp. 65–75,
1046 doi:10.1029/143GM05.
1047 Cannon, E.C. and Bürgmann, R., 2001. Prehistoric fault offsets of the Hilina fault system, south
1048 flank of Kilauea Volcano, Hawaii. J. Geophys. Res., 106(B3): 4207–4219,
1049 doi:10.1029/2000JB900412.
1050 Cannon, E.C., Bürgmann, R. and Owen, S.E., 2001. Shallow normal faulting and block rotation
1051 associated with the 1975 Kalapana earthquake, Kilauea Volcano, Hawaii. Bull. Seismol. Soc.
1052 Am., 91(6): 1553–1562, doi:10.1785/0120000072.
1053 Carracedo, J.C., 1999. Growth, structure, instability and collapse of Canarian volcanoes and
1054 comparisons with Hawaiian volcanoes. J. Volcanol. Geotherm. Res., 94(1): 1–19,
1055 doi:10.1016/S0377-0273(99)00095-5.

Carracedo, J.C., Day, S.J., Guillou, H., Torrado, F.J.P., 1999. Giant quaternary landslides in the evolution of La Palma and El Hierro, Canary Islands. J. Volcanol. Geotherm. Res., 94(1): 169–190, doi:10.1016/S0377-0273(99)00102-X.

Cayol, V., Catry, T., Michon, L., Chaput, M., Famin, V., Bodart, O., Froger, J.-L. and Romagnoli, C., 2014. Sheared sheet intrusions as a mechanism for lateral flank displacement on basaltic volcanoes: Applications to Réunion Island volcanoes. J. Geophys. Res., 119(10): 7607–7635, doi:10.1002/2014JB011139.

Cervelli, P., Segall, P., Johnson, K., Lisowski, M. and Miklius, A., 2002a. Sudden aseismic fault slip on the south flank of Kilauea volcano. Nature, 415(6875): 1014-1018, doi:10.1038/4151014a.

Cervelli, P., Segall, P., Amelung, F., H., G., Owen, S., Miklius, A. and Lisowski, M., 2002b. The 12 September 1999 Upper East Rift Zone dike intrusion at Kilauea Volcano, Hawaii. J. Geophys. Res., 107(B7): doi:10.1029/2001JB000602.

Chadwick, W.W., Jr. and Dieterich, J.H., 1995. Mechanical modeling of circumferential and radial dike intrusion on Galapagos volcanoes. J. Volcanol. Geotherm. Res., 66(1–4): 37–52, doi:10.1016/0377-0273(94)00060-T.

Chaput, M., Pinel, V., Famin, V., Michon, L., Froger, J.-L., 2014, Cointrusive shear displacement by sill intrusion in a detachment: A numerical approach. Geophys. Res. Lett., 41(6): 1937–1943, doi:10.1002/2013GL058813.

Chen, Y, Remy, D., Froger, J-L., Peltier, A., Villeneuve, N., Darrozes, J., Perfettini, H., Bonvalot, S., in revision. Long-term ground displacement observed by InSAR and GNSS at Piton de la Fournaise volcano between 2009 and 2014. Rem. Sens. Environ..

Chiocci, F.L., Coltelli, M., Bosman, A., Cavallaro, D., 2011. Continental margin large-scale instability controlling the flank sliding of Etna volcano. Earth Planet. Sci. Lett., 305(1–2): 57–64, doi:10.1016/j.epsl.2011.02.040.

Clague, D.A., and Dalrymple, G.B., 1987. The Hawaiian-Emperor volcanic chain; part 1. Geologic evolution. In: Decker, R.W., Wright, T.L., Stauffer, P.H. (Eds.), Volcanism in Hawaii. U.S. Geol. Surv. Prof. Pap. 1350, pp. 5–54.

Clague, D.A. and Denlinger, R.P., 1994. Role of olivine cumulates in destabilizing the flanks of Hawaiian volcanoes. Bull. Volcanol., 56(6–7): 425–434, doi:10.1007/BF00302824.

Clague, D.A. and Sherrod, D.R., 2014. Growth and degradation of Hawaiian Volcanoes. In: Poland, M.P., Landowski, C.M., Takahashi, T.J. (Eds.), Characteristics of Hawaiian Volcanoes. U.S. Geol. Surv. Prof. Pap. 1801, pp. 97–146, doi:10.3133/pp18013.

Clarke, D., Brenguier, F., Froger, J.-L., Shapiro, N.M., Peltier, A., Staudacher, T., 2013. Timing of a large volcanic flank movement at Piton de la Fournaise Volcano using noise-based seismic monitoring and ground deformation measurements. Geophys. J. Int., 195(2): 1132–1140, doi:10.1093/gji/ggt276.

Courteaud, M., 1996. Etude des structures géologiques et hydrogéologiques du massif de la Fournaise par la méthode audiomagnétotellurique. Ph.D. Dissertation, Université de la Réunion, 212 pp.

Day, S.J., Da Silva, S.H. and Fonseca, J.F.B.D., 1999. A past giant lateral collapse and present-day flank instability of Fogo, Cape Verde Islands. J. Volcanol. Geotherm. Res., 94(1): 191–218, doi:10.1016/S0377-0273(99)00103-1.

De Gori, P., Chiarabba, C., Patanè, D., 2005. Qp structure of Mount Etna: Constraints for the physics of the plumbing system. J. Geophys. Res., 110(5): doi:10.1029/2003JB002875.

Del Carlo, P., Vezzoli, L., Coltelli, M., 2004. Last 100 ka Tephrostratigraphic record of Mount

Etna. In: Bonaccorso A., Calvari S., Coltelli M., Del Negro C., Falsaperla S. (Eds.), Mt. Etna Volcano Laboratory. Am. Geoph. Union Geophys. Mono., 143, pp. 77–89, doi:10.1029/143GM06.

Delaney, P.T., Fiske, R.S., Miklius, A., Okamura, A.T. and Sako, M.K., 1990. Deep magma body beneath the summit and rift zones of Kilauea Volcano, Hawaii. Science, 247(4948): 1311–1316, doi:10.1126/science.247.4948.1311.

Denlinger, R.P. and Morgan, J.K., 2014. Instability of Hawaiian Volcanoes. In: Poland, M.P., Landowski, C.M., Takahashi, T.J. (Eds.), Characteristics of Hawaiian Volcanoes. U.S. Geol. Surv. Prof. Pap. 1801, pp. 149–176, doi:10.3133/pp18014.

Derrien, A., Villeneuve, N., Peltier, A., Beauducel, F., 2015. Retrieving 65 years of volcano summit deformation from multitemporal structure from motion: The case of Piton de la Fournaise (La Réunion Island). Geophys. Res. Lett. 42(17): 6959–6966, doi:10.1002/2015GL064820.

Di Muro, A., Métrich, N., Vergani, D., Rosi, M., Armienti, P., Fougeroux, T., Deloule, E., Arienzo, I., Civetta, L., 2014. The Shallow Plumbing System of Piton de la FournaiseVolcano (La Réunion Island, Indian Ocean) Revealed by the Major 2007 Caldera-Forming Eruption. J Petrol. 55(7): 1287–1315, doi:10.1093/petrology/egu025.

Di Traglia, F., Intrieri, E., Nolesini, T., Bardi, F., Del Ventisette, C., Ferrigno, F., Frangioni, S., Frodella, W., Gigli, G., Lotti, A., Tacconi Stefanelli, C., Tanteri, L., Leva, D., Casagli, N., 2014. The ground-based InSAR monitoring system at Stromboli volcano: linking changes in displacement rate and intendity of persistent volcanic activity. Bull. Volcanol., 76: 786, doi:10.1007/s00445-013-0786-2.

Dieterich, J.H., 1988. Growth and persistence of Hawaiian volcanic rift zones. J. Geophys. Res., 93(B5): 4258–4270, doi:10.1029/JB093iB05p04258.

Duffield, W.A., 1975. Structure and Origin of the Koae Fault System, Kilauea Volcano, Hawaii. U.S. Geol. Surv. Prof. Pap. 856, 12 pp.

Duncan, R. A., 1981. Hotspots in the southern oceans: An absolute frame of reference for motion of the Gondwana continents. Tectonophys, 74(1–2): 29−24, doi:10.1016/0040-1951(81)90126-8.

Dzurisin, D., Anderson, L.A., Eaton, G.P., Koyanagi, R.Y., Lipman, P.W., Lockwood, J.P., Okamura, R.T., Puniwai, G.S., Sako, M.K. and Yamashita, K.M., 1980. Geophysical observations of Kilauea Volcano, Hawaii; 2, Constraints on the magma supply during November 1975-September 1977. J. Volcanol. Geotherm. Res., 7(3–4): 241–269, doi:10.1016/0377-0273(80)90032-3.

Famin, V. and Michon, L., 2010. Volcano destabilization by magma injections in a detachment. Geology, 38(3): 219–222, doi:10.1130/G30717.1.

Fernández, J., Tizzani, P., Manzo, M., Borgia, A., González, P.J., Martí, J., Pepe, A., Camacho, A.G., Casu, F., Berardino, P., Prieto, J.F. and Lanari, R., 2009. Gravity-driven deformation of Tenerife measured by InSAR time series analysis. Geophys. Res. Lett., 36(4): doi:10.1029/2008GL036920.

Froger, J.L., Merle, O., Briole, P., 2001. Active spreading and regional extension at Mount Etna imaged by SAR interferometry. Earth Planet. Sci. Lett., 187(3): 245–258, doi:10.1016/S0012-821X(01)00290-4.

Froger, J.-L, Famin, V., Cayol, V., Augier, A., Michon, L., Lénat, J.-L., 2015. Time-dependent displacements during and after the April 2007 eruption of Piton de la Fournaise, revealed by interferometric data. J. Volcanol. Geotherm. Res. 296: 55–68,

1148 doi:10.1016/j.jvolgeores.2015.02.014.
1149 Gailler, L.-S, Lénat, J.-F., Lambert, M., Levieux, G., Villeneuve, N., Froger, J.-L., 2009. Gravity
1150 structure of Piton de la Fournaise volcano and inferred mass transfer during the 2007 crisis.
1151 J. Volcanol. Geotherm. Res. 184(1–2): 31–48, doi:10.1016/j.jvolgeores.2009.01.024.
1152 Gambino, S., Bonforte A., Carnazzo A., Falzone G., Ferrari F., Ferro, A., Guglielmino F.,
1153 Laudani G., Maiolino, V., Puglisi G., 2011. Displacement across the Trecastagni Fault (Mt.
1154 Etna) and induced seismicity: The October 2009 to January 2010 episode. Ann. Geophys.,
1155 54(4): doi:10.4401/ag-4841.
1156 Geist, D., White, W.M., Albarede, F., Harpp, K., Reynolds, R., Blichert-Toft, J. and Kurz, M.,
1157 2002. Volcanic evolution in the Galapagos: The dissected shield of Volcan Ecuador.
1158 Geochem., Geophys., Geosys., 3(10): doi:10.1029/2002GC000355.
1159 Geist, D., Chadwick, W. and Johnson, D., 2006. Results from new GPS and gravity monitoring
1160 networks at Fernandina and Sierra Negra Volcanoes, Galápagos, 2000–2002. J. Volcanol.
1161 Geotherm. Res., 150(1–3): 79–97, doi:10.1016/j.jvolgeores.2005.07.003.
1162 Gillot, P.- Y., Nativel, P., 1989. Eruption history of the Piton de la Fournaise volcano, Reunion
1163 Island, Indian Ocean. J. Volcanol. Geotherm. Res. 36(1–3): 53−65, doi:10.1016/0377-
1164 0273(89)90005-X.
1165 González, P.J., Tiampo, K.F., Camacho, A.G. and Fernández, J., 2010. Shallow flank
1166 deformation at Cumbre Vieja volcano (Canary Islands): Implications on the stability of steep-
1167 sided volcano flanks at oceanic islands. Earth Planet. Sci. Lett., 297(3–4): 545–557,
1168 doi:10.1016/j.epsl.2010.07.006.
1169 González, P.J., Samsonov, S.V., Pepe, S., Tiampo, K.F., Tizzani, P., Casu, F., Fernández, J.,
1170 Camacho, A.G. and Sansosti, E., 2013. Magma storage and migration associated with the
1171 2011–2012 El Hierro eruption: implications for crustal magmatic systems at oceanic island
1172 volcanoes. J. Geophys. Res., 118(8): 4361–4377, doi:10.1002/jgrb.50289.
1173 González, P.J., Bagnardi, M., Hooper, A.J., Larsen, Y., Marinkovic, P., Samsonov, S.V. and
1174 Wright, T.J., 2015. The 2014-2015 eruption of Fogo volcano: geodetic modelling of
1175 Sentinel-1 TOPS interferometry. Geophysical Research Letters, 42(21): 9239–9246,
1176 doi:10.1002/2015GL066003.
1177 Got., J.-L., and Okubo, P.G., 2003. New insights into Kilauea's volcano dynamics brought by
1178 large-scale relative relocation of microearthquakes. J. Geophys. Res., 108(B7):
1179 doi:10.1029/2002JB002060
1180 Got, J. L., Peltier, A., Staudacher, T., Kowalski, P., Boissier, P., 2013. Edifice strength and
1181 magma transfer modulation at Piton de la Fournaise volcano. J. Geophys. Res., 118(9):
1182 5040–5057, doi:10.1002/jgrb.50350.
1183 Gripp, A.E. and Gordon, R.G., 2002. Young tracks of hotspots and current plate velocities.
1184 Geophys. J. Int., 150(2): 321–361, doi:10.1046/j.1365-246X.2002.01627.x.
1185 Gross, F., Krastel, S., Geersen,J., Behrmann, J.H., Ridente, D., Chiocci, F., Bialas, J.,Papenberg,
1186 C., Cukur, D., Urlaub, M., Micallef, A., 2015. The limits of seaward spreading and slope
1187 instability at the continental margin offshore Mt Etna, imaged by high-resolution 2D
1188 seismic data. Tectonophys., 667: 63–76, doi:10.1016/j.tecto.2015.11.011.
1189 Guglielmino, F., Bignami, C., Bonforte, A., Briole, P., Obrizzo, F., Puglisi, G., Stramondo, S.,
1190 Wegmuller U., 2011. Analysis of satellite and in situ ground deformation data integrated
1191 by the SISTEM approach: The April 3, 2010 earthquake along the Pernicana fault (Mt.
1192 Etna - Italy) case study. Earth Planet. Sci. Lett., 312(3–4): 327–336,
1193 doi:10.1016/j.epsl.2011.10.028.

1194 Harris, A. J. L., Steffke, A., Calvari, S., and Spampinato, L., 2011. Thirty years of satellite-
1195 derived lava discharge rates at Etna: Implications for steady volumetric output. J. Geophys.
1196 Res., 116(B08): doi:10.1029/2011JB008237.
1197 Harris, A. J. L., Steffke, A., Calvari, S., and Spampinato, L., 2012. Correction to "Thirty years of
1198 satellite-derived lava discharge rates at Etna: Implications for steady volumetric output". J.
1199 Geophys. Res., 117(B08): doi:10.1029/2012JB009431.
1200 Hildenbrand, A., Marques, F.O., Catalão, J., Catita, C.M.S., and Costa, A.C.G., 2012. Large-
1201 scale active slump of the southeastern flank of Pico Island, Azores. Geology, 40(10): 939 –
1202 942, doi: 10.1130/G33303.1.
1203 Hirn, A., Nicolich, R., Gallart, J., Laigle, M., Cernobori, L., ETNASEIS Scientific Group, 1997.
1204 Roots of Etna volcano in faults of great earthquakes. Earth Plan. Sci. Lett. 148(1–2): 171–
1205 191, doi:10.1016/S0012-821X(97)00023-X.
1206 Holcomb, R.T. and Searle, R.C., 1991. Large landslides from oceanic volcanoes. Marine
1207 Geotech., 10(1–2): 19–32, doi:10.1080/10641199109379880.
1208 Houliè, N., Briole, P., Bonforte, A., Puiglisi, G., 2006. Large scale ground deformation of Etna
1209 observed by GPS between 1994 and 2001. Geophys. Res. Lett., 33(2):
1210 doi:10.1029/2005GL024414.
1211 Hürlimann, M., Garcia-Piera, J.O., Ledesma, A., 2000. Causes and mobility of large volcanic
1212 landslides: application to Tenerife, Canary Islands. J. Volcanol. Geotherm. Res., 103(1):
1213 121–134, doi:10.1016/S0377-0273(00)00219-5.
1214 Iverson, R.M., 1995. Can magma-injection and groundwater forces cause massive landslides on
1215 Hawaiian volcanoes? J. Volcanol. Geotherm. Res., 66(1–4): 295–308, doi:10.1016/0377-
1216 0273(94)00064-N.
1217 Johnson, J.H., Swanson, D.A., Roman, D.C., Poland, M.P. and Thelen, W.A., 2015. Crustal
1218 stress and structure at Kīlauea Volcano inferred from seismic anisotropy. In: Carey, R.J.,
1219 Cayol, V., Poland, M.P., Weis, D. (Eds.), Hawaiian Volcanoes, From Source to Surface. Am.
1220 Geophys. Un. Geophys. Mono., 208, pp. 251–268, doi:10.1002/9781118872079.ch12.
1221 Kauahikaua, J. and Miklius, A., 2003. Long-term trends in microgravity at Kilauea's summit
1222 during the Pu`u `O`o-Kupianaha eruption. In: Heliker, C., Swanson, D.A., Takahashi, T.J.
1223 (Eds.), The Puʻu ʻŌʻō-Kupaianaha Eruption of Kilauea Volcano, Hawaii: The First 20 Years,
1224 U.S. Geol. Surv. Prov. Pap. 1676, pp. 165–171.
1225 Krastel, S., Schmincke, H.U., Jacobs, C.L., Rihm, R., Le Bas, T.P. and Alibés, B., 2001.
1226 Submarine landslides around the Canary Islands. J. Geophys. Res., 106(B3): 3977–3997,
1227 doi:10.1029/2000JB900413.
1228 Laigle, M., Hirn, A., Sapin, M., Lépine, J.C., Diaz, J., Gallart, J., Nicolich, R., 2000. Mount Etna
1229 dense array local earthquake P and S tomography and implications for volcanic plumbing.
1230 J. Geophys. Res. 105(B9): 21633–21646, doi:10.1029/2000JB900190.
1231 Labazuy, P., 1996. Recurrent landslides events on the submarine flank of Piton de la Fournaise
1232 volcano (Réunion Island). In: McGuire, W.J., Jones, A.P., Neuberg, J. (Eds.), Volcano
1233 Instability on the Earth and Other Planets. Geol. Soc. Spec. Publ., 110, pp. 293-305.
1234 Le Corvec, N., Walter, T.R., Ruch, J., Bonforte, A., Puglisi, G., 2014. Experimental study of the
1235 interplay between magmatic rift intrusion and flank instability with application to the 2001
1236 Mount Etna eruption. J. Geophys. Res., 119(7): 5356–5368, doi:10.1002/2014JB011224.
1237 Le Friant, A., Lebas, E., Clément, V., Boudon, G., Deplus, C., de Voogd, B., Bachèlery, P.,
1238 2011. A new model for the evolution of la Réunion volcanic complex from complete
1239 marine geophysical surveys. Geophys. Res. Lett. 38(9): doi:10.1029/2011GL047489.

Lénat, J.- F., Bachèlery, P., Bonneville, A., Galdéano, A., Labazuy, P., Rousset, D., Vincent, P., 1990. Structure and morphology of the submarine flank of an active basaltic volcano: Piton de La Fournaise (Reunion Island, Indian Ocean). Oceanol. Acta, 10: 211–223.

Lentini, F., Carbone, S., Guarnieri, P., 2006. Collisional and postcollisional tectonics of the Apenninic-Maghrebian orogen (southern Italy). In: Dilek, Y., Pavlides, S. (Eds.), Postcollisional tectonics and magmatism in the Mediterranean region and Asia, Geol. Soc. Am. Sp. Pap. 409, pp. 57–81, doi:10.1130/2006.2409(04).

Lipman, P.W. and Calvert, A.T., 2013. Modeling volcano growth on the Island of Hawaii: Deep-water perspectives. Geosphere, 9(5): 1348–1383, doi:10.1130/GES00935.1.

Lipman, P.W., Lockwood, J.P., Okamura, R.T., Swanson, D.A. and Yamashita, K.M., 1985. Ground deformation associated with the 1975 Magnitude-7.2 earthquake and resulting changes in activity of Kilauea Volcano, Hawaii. U.S. Geol. Surv. Prof. Pap. 1276, 45 pp.

Lo Giudice E. and Rasà R., 1992. Very shallow earthquakes and brittle deformations in active volcanic areas: the Etnean region as an example. Tectonophysics, 202: 257–268, doi:10.1016/0040-1951(92)90111-I.

Lundgren, P., Poland, M., Miklius, A., Orr, T., Yun, S.-H., Fielding, E., Liu, Z., Tanaka, A., Szeliga, W., Hensley, S. and Owen, S., 2013. Evolution of dike opening during the March 2011 Kamoamoa fissure eruption, Kīlauea Volcano, Hawai‘i. J. Geophys. Res., 118(3): 897–914, doi:10.1002/jgrb.50108.

Masson, D.G., Watts, A.B., Gee, M.J.R., Urgeles, R., Mitchell, N.C., Le Bas, T.P. and Canals, M., 2002. Slope failures on the flanks of the western Canary Islands. Earth Sci. Rev., 57(1): 1–35, doi:10.1016/S0012-8252(01)00069-1.

Mathieu, L., Kervyn, M. and Ernst, G.G.J., 2011. Field evidence for flank instability, basal spreading and volcano-tectonic interactions at Mt Cameroon, West Africa. Bull. Volcanol., 73(7): 851–867, doi:10.1007/s00445-011-0458-z.

Matoza, R.S., Shearer, P.M., Lin, G., Wolfe, C.J. and Okubo, P.G., 2013. Systematic relocation of seismicity on Hawaii Island from 1992 to 2009 using waveform cross-correlation and cluster analysis. J. Geophys. Res., 118(5): 2275–2288, doi:10.1002/jgrb.50189.

Mattia, M., Bruno, V., Caltabiano, T., Cannata, A., Cannavò, F., D'Alessandro, W., Di Grazia, G., Federico, C., Giammanco, S., La Spina, A., Liuzzo, M., Longo, M., Monaco, C., Patané, D., and Salerno, G., 2015. A comprehensive interpretative model of slow slip events on Mt. Etna's eastern flank: Geochem. Geophys. Geosyst., 16: 635–658, doi:10.1002/2014GC005585.

McGuire, W.J., Moss, J.L., Saunders, S.J., Stewart, I.S., 1996. Dyke induced rifting and edifice instability at Mount Etna. In: Gravestock, P.J., Mc Guire, W.J. (Eds.), Etna: Fifteen years on. Cheltenham and Gloucester Sp. Publ., pp. 20–24.

Merle, O. and Borgia, A., 1996. Scaled experiments of volcanic spreading. J. Geophys. Res., 101(B6): 13,805–13,817, doi:10.1029/95JB03736.

Merle, O. and Lénat, J.F., 2003. Hybrid collapse mechanism at Piton de la Fournaise volcano, Reunion Island, Indian Ocean. J. Geophys. Res, 108, 2166, doi:10.1029/2002JB002014.

Michon, L. and Saint-Ange, F., 2008. Morphology of Piton de la Fournaise basaltic shield volcano (La Réunion Island): Characterization and implication in the volcano evolution. J. Geophys. Res., 113(B3): doi:10.1029/2005JB004118.

Michon, L., Saint-Ange, F., Bachèlery, P., Villeneuve, N., Staudacher, T., 2007. Role of the structural inheritance of the oceanic lithosphere in the magmato- tectonic evolution of

Piton de la Fournaise volcano (La Réunion Island). J. Geophys. Res. 112(B4): doi:10.1029/2006JB004598.
Michon, L., Di Muro, A., Villeneuve, N., Saint-Marc, C., Fadda, P., Manta, F., 2013. Explosive activity of the summit cone of Piton de la Fournaise volcano (La Réunion island): A historical and geological review. J. Volcanol. Geotherm. Res., 263: 117–133, doi:10.1016/j.jvolgeores.2013.06.012.
Michon, L., Ferrazzini, V., Di Muro, A., Villeneuve, N., Famin, V., 2015. Rift zones and magma plumbing system of Piton de la Fournaise volcano: How do they differ from Hawaii and Etna? J. Volcanol. Geotherm. Res. 303: 112–129, doi:10.1016/j.jvolgeores.2015.07.031.
Miklius, A., Lisowski, M., Delaney, P.T., Denlinger, R.P., Dvorak, J.J., Okamura, A.T., and Sako, M.K., 1995. Recent inflation and flank movement of Mauna Loa volcano. In: Rhodes, J.M., Lockwood, J.P. (Eds.), Mauna Loa Revealed: Structure, Composition, History, and Hazards. Am. Geophys. Un. Geophys. Mono., pp.199–205, doi:10.1029/GM092p0199.
Miklius, A., Cervelli, P., Sako, M., Lisowski, M., Owen, S., Segall, P., Foster, J., Kamibayashi, K. and Brooks, B., 2005. Global Positioning System Measurements on the Island of Hawai`i: 1997 through 2004. U.S. Geol. Surv. Open-File Rep., 2005–1425, 46 pp.
Montgomery-Brown, E.K., Segall, P. and Miklius, A., 2009. Kilauea slow slip events: Identification, source inversions, and relation to seismicity. J. Geophys. Res., 114(B6): doi:10.1029/2008JB006074.
Montgomery-Brown, E.K., Sinnett, D.K., Poland, M., Segall, P., Orr, T., Zebker, H. and Miklius, A., 2010. Geodetic evidence for en echelon dike emplacement and concurrent slow-slip during the June 2007 intrusion and eruption at Kīlauea volcano, Hawaii. J. Geophys. Res., 115(B7): doi:10.1029/2009JB006658.
Montgomery-Brown, E.K., Poland, M.P. and Miklius, A., 2015. Delicate balance of magmatic-tectonic interaction at Kīlauea Volcano, Hawai‘i, revealed from slow slip events. In: Carey, R.J., Cayol, V., Poland, M.P., Weis, D. (Eds.), Hawaiian Volcanoes, From Source to Surface. Am. Geophys. Un. Geophys. Mono., 208, pp. 269–288, doi:10.1002/9781118872079.ch13.
Moore, J.G., 1964. Giant submarine landslides on the Hawaiian Ridge. U.S. Geol. Surv. Prof. Pap. 501-D., pp. D95–D98.
Moore, J.G. and Krivoy, H.L., 1964. The 1962 flank eruption of Kilauea Volcano and structure of the east rift zone. J. Geophys. Res., 69(10): 2033–2045, doi:10.1029/JZ069i010p02033.
Moore, J. G., Clague, D. A., Holcomb, R. T., Lipman, P. W., Normark, W. R., Torresan, M. E., 1989. Prodigious submarine landslides on the Hawaiian Ridge, J. Geophys. Res. 94(B12): 17,465–17,848, doi:10.1029/JB094iB12p17465.
Morgan, J.K., Moore, G.F., Hills, D.J. and Leslie, S., 2000. Overthrusting and sediment accretion along Kilauea's mobile south flank, Hawaii: Evidence for volcanic spreading from marine seismic reflection data. Geology, 28(7): 667–670, doi:10.1130/0091-7613(2000)28<667:OASAAK>2.0.CO;2.
Morgan, W.J., 1981. Hotspot tracks and the opening of the Atlantic and Indian Oceans. In: Emiliani, C. (ed.), The Sea. Wiley, New York, pp. 443−487.
Münn, S., Walter, T.R., and Klügel, A., 2006. Gravitational spreading controls rift zones and flank instability on El Hierro, Canary Islands. Geol. Mag., 143(3): 257–268, doi:10.1017/S0016756806002019.
Nakamura, K., 1980, Why do long rift zones develop in Hawaiian volcanoes: A possible role of thick oceanic sediments. Bull. Volcanol. Soc. Japan, 25: 255–269 (in Japanese, with English Abstr.).

1331 Neri, M., Guglielmino, F., Rust, D., 2007. Flank instability on Mount Etna: Radon, radar
1332 interferometry and geodetic data from the southwestern boundary of the unstable sector, J.
1333 Geophys. Res., 112(B4): doi:10.1029/2006JB004756.
1334 Norini, G. and Acocella, V., 2011. Analogue modeling of flank instability at Mount Etna:
1335 understanding the driving factors. J. Geophys. Res., 116(B7), doi:10.1029/2011JB008216.
1336 Oehler, J.F., Labazuy, P., Lénat, J.F., 2004. Recurrence of major flank landslides during the last
1337 2-Ma-history of Reunion Island. Bull. Volcanol., 66(7): 585–598, doi:10.1007/s00445-
1338 004-0341-2.
1339 Oehler, J.F., van Wyk de Vries, B., Labazuy, P., 2005. Landslides and spreading of oceanic
1340 hotspot and arc shield volcanoes on Low Strength Layers (LSLs): An analogue modelling
1341 approach. J. Volcanol. Geotherm. Res., 144(1–4): 169–189,
1342 doi:10.1016/j.jvolgeores.2004.11.023.
1343 Oehler, J.F., Lénat, J.F., Labazuy, P., 2008. Growth and collapse of the Reunion Island
1344 volcanoes, Bull. Volcanol. 70(6): 717–742, doi:10.1007/s00445- 007- 0163- 0.
1345 Orr, T.R., Poland, M.P., Patrick, M.R., Thelen, W.A., Sutton, A.J., Elias, T., Thornber, C.R.,
1346 Parcheta, C. and Wooten, K.M., 2015. Kīlauea's 5–9 March 2011 Kamoamoa fissure eruption
1347 and its relation to 30+ years of activity from Pu‘u ‘Ō ‘ō. In: Carey, R.J., Cayol, V., Poland,
1348 M.P., Weis, D. (Eds.), Hawaiian Volcanoes, From Source to Surface. Am. Geophys. Un.
1349 Geophys. Mono., 208, pp. 393–420, doi:10.1002/9781118872079.ch18.
1350 Owen, S., Segall, P., Freymueller, J.T., Miklius, A., Denlinger, R.P., Arnadottir, T., Sako, M.K.
1351 and Bürgmann, R., 1995. Rapid deformation of the south flank of Kilauea Volcano, Hawaii.
1352 Science, 267(5202): 1328–1332, doi:10.1126/science.267.5202.1328.
1353 Owen, S., Segall, P., Lisowski, M., Miklius, A., Denlinger, R. and Sako, M., 2000a. Rapid
1354 deformation of Kilauea Volcano: Global Positioning System measurements between 1990
1355 and 1996. J. Geophys. Res., 105(B8): 18,983-18,993, doi:10.1029/2000JB900109.
1356 Owen, S., Segall, P., Lisowski, M., Miklius, A., Murray, M., Bevis, M. and Foster, J., 2000b.
1357 January 30, 1997 eruptive event on Kilauea Volcano, Hawaii, as monitored by continuous
1358 GPS. Geophysical Research Letters, 27(17): 2757–2760, doi:10.1029/1999GL008454.
1359 Patanè, D., De Gori, P., Chiarabba, C., Bonaccorso, A., 2003. Magma ascent and the
1360 pressurization of Mount Etna’s volcanic system. Science, 299(5615), 2061–2063,
1361 doi:10.1126/science.1080653.
1362 Patanè, G., Montalto, A.,. Imposa, S., Menza, S., 1994. The role of regional tectonics, magma
1363 pressure and gravitational spreading in earthquakes of the eastern sector of Mt. Etna
1364 volcano (Italy). J. Volcanol. Geotherm. Res., 61(3–4): 253–266, doi:10.1016/0377-
1365 0273(94)90007-8.
1366 Peltier, A., Staudacher, T., Bachèlery, P., 2007. Constraints on magma transfers and structures
1367 involved in the 2003 activity at Piton de La Fournaise from displacement data. J. Geophys.
1368 Res., 112(B3): doi:10.1029/2006JB004379.
1369 Peltier, A., Famin, V., Bachèlery, P., Cayol, V., Fukushima, Y., Staudacher, T., 2008. Cyclic
1370 magma storages and transfers at Piton de La Fournaise volcano (La Réunion hotspot)
1371 inferred from deformation and geochemical data. Earth Planet. Sci. Lett. 270(3–4): 180–
1372 188, doi:10.1016/j.epsl.2008.02.042.
1373 Peltier, A., Bachèlery, P., Staudacher, T., 2009. Magma transfer and storage at Piton de La
1374 Fournaise (La Réunion Island) between 1972 and 2007: A review of geophysical and
1375 geochemical data. J. Volcanol. Geotherm. Res. 184(1–2), 93–108,
1376 doi:10.1016/j.jvolgeores.2008.12.008.

Peltier, A., Massin, F., Bachèlery, P., Finizola, A., 2012. Internal structures and building of basaltic shield volcanoes: The example of the Piton de La Fournaise terminal cone (La Réunion). Bull. Volcanol. 74(8): 1881–1897, doi:10.1007/s0044501206367.

Peltier, A., Poland, M.P., Staudacher, T., 2015a. Are Piton de la Fournaise (La Réunion) and Kīlauea (Hawai‘i) Really "Analog Volcanoes. In: Carey, R.J., Cayol, V., Poland, M.P., Weis, D. (Eds.), Hawaiian Volcanoes, From Source to Surface. Am. Geophys. Un. Geophys. Mono., 208, pp. 507–531, doi:10.1002/9781118872079.ch23.

Peltier, A., Got, J.-L., Villeneuve, N., Boissier, P., Staudacher, T., Ferrazzini, V., Walpersdorf, A., 2015b. Long-term mass transfer at Piton de la Fournaise volcano evidenced by strain distribution derived from GNSS network. J. Geophys. Res., 120(3): 1874–1889, doi:10.1002/2014JB011738.

Peltier, A., Beauducel, F., Villeneuve, N., Ferrazzini, V., Di Muro, A., Aiuppa, A., Derrien, A., Jourde, K., Taisne, B., 2016. Deep fluid transfer evidenced by surface deformation during the 2014-2015 unrest at Piton de la Fournaise volcano. J. Volcanol. Geotherm. Res., 321: 140–148, doi :10.1016 :j.jvolgeores.2016.04.031.

Phillips, K.A., Chadwell, C.D. and Hildebrand, J.A., 2008. Vertical deformation measurements on the submerged south flank of Kilauea volcano, Hawai'i reveal seafloor motion associated with volcanic collapse. J. Geophys. Res., 113(5): doi:10.1029/2007JB005124.

Plattner, C., Amelung, F., Baker, S., Govers, R. and Poland, M.P., 2013. The role of viscous magma mush spreading in volcanic flank motion at Kīlauea Volcano, Hawai'i. J. Geophys. Res., 118(5): 2474–2487, doi:10.1002/jgrb.50194.

Poland, M.P., 2014a. Contrasting Volcanism in Hawai‘i and the Galápagos. In: Harpp, K.S., Mittelstaedt, E., d'Ozouville, N., Graham, D.W. (Eds.), The Galápagos: A Natural Laboratory for the Earth Sciences. Am. Geophys. Un. Geophys. Mono., 204, pp. 5-26, doi:10.1002/9781118852538.ch2.

Poland, M.P., 2014b. Time-averaged discharge rate of subaerial lava at Kīlauea Volcano, Hawai‘i, measured from TanDEM-X interferometry: Implications for magma supply and storage during 2011–2013. J. Geophys. Res., 119(7): 5464–5481, doi:10.1002/2014JB011132.

Poland, M.P., Miklius, A., Orr, T., Sutton, A.J., Thornber, C.R. and Wilson, D., 2008. New episodes of volcanism at Kilauea Volcano, Hawaii. EOS Trans. Am. Geophys. Un., 89(5): 37–38, doi:10.1029/2008EO050001.

Poland, M.P., Miklius, A., Sutton, A.J. and Thornber, C.R., 2012. A mantle-driven surge in magma supply to Kīlauea Volcano during 2003–2007. Nature Geosci., 5(4): 295–300, doi:10.1038/ngeo1426.

Poland, M.P., Miklius, A. and Montgomery-Brown, E.K., 2014. Magma supply, storage, and transport at shield-stage Hawaiian volcanoes. In: Poland, M.P., Landowski, C.M., Takahashi, T.J. (Eds.), Characteristics of Hawaiian Volcanoes. U.S. Geol. Surv. Prof. Pap. 1801, pp. 179–234, doi:10.3133/pp18015.

Prôno, E., Battaglia, J., Monteiller, V., Got, J.-L., Ferrazzini, V., 2009. P-wave velocity structure of Piton de la Fournaise volcano deduced from seismic data recorded between 1996 and 1999. J. Volcanol. Geotherm. Res. 184(1–2): 49–62, doi:10.1016/j.jvolgeores.2008.12.009.

Puglisi, G., Bonforte, A., Maugeri, S.R., 2001. Ground deformation patterns on Mt. Etna, 1992 to 1994, inferred from GPS data. Bull. Volcanol., 62(6): 371–384 doi:10.1007/s004450000112.

Puglisi, G., Bonforte, A., Ferretti, A., Guglielmino, F., Palano, M., Prati, C., 2008. Dynamics of

Mount Etna before, during, and after the July–August 2001 eruption inferred from GPS and differential synthetic aperture radar interferometry data. J. Geophys. Res., 113(B6): doi:10.1029/2006JB004811.

Robinson, J.E. and Eakins, B.W., 2006. Calculated volumes of individual shield volcanoes at the young end of the Hawaiian Ridge. J. Volcanol. Geotherm. Res., 151(1–3): 309–317, doi:10.1016/j.jvolgeores.2005.07.033.

Roult, G., Peltier, A., Taisne, B., Staudacher, T., Ferrazzini, V., Di Muro, A., the OVPF team, 2012. A new comprehensive classification of the Piton de la Fournaise activity spanning the 1985–2010 period: Search and analysis of short-term precursors from a broad-band seismological station. J. Volcanol. Geotherm. Res., 241–242: 78–104, doi:10.1016/j.jvolgeores.2012.06.012.

Ruch, J., Acocella, V., Storti, F., Neri, M., Pepe, S., Solaro, G., Sansosti, E., 2010. Detachment depth revealed by rollover deformation: An integrated approach at Mount Etna. Geophys. Res. Lett., 37, L16304, doi:10.1029/2010GL044131.

Ruch, J., Pepe, S., Casu, F., Acocella, V., Neri, M., Solaro, G., Sansosti, E., 2012. How do volcanic rift zones relate to flank instability? Evidence from collapsing rifts at Etna. Geophys. Res. Lett., 39, L20311, doi:10.1029/2012GL053683.

Ruch, J., Pepe, S., Casu, F., Solaro, G., Pepe, A., Acocella, V., Neri, M., Sansosti, E., 2013. Seismo-tectonic behavior of the Pernicana Fault System (Mt Etna): A gauge for volcano flank instability? J. Geophys. Res., 118(8): 4398–4409, doi:10.1002/jgrb.50281.

Rust, D. and Neri, M., 1996. The boundaries of large- scale collapse on the flanks of Mount Etna, Sicily. In: McGuire, W.J., Jones, A.P., Neuberg, J. (Eds.), Volcano Instability on the Earth and Other Planets. Geol. Soc. Spec. Publ., 110, pp. 193–208.

Saint‐Ange, F., Bachèlery, P., Babonneau, N., Michon, L., Jorry, S.J., 2013. Volcaniclastic sedimentation on the submarine slopes of a basaltic hotspot volcano: Piton de la Fournaise volcano (La Réunion Island, Indian Ocean). Marine Geol. 337: 35–52, doi:10.1016/j.margeo.2013.01.004.

Schaefer, L.N., Lu, Z. and Oommen, T., 2015. Dramatic volcanic instability revealed by InSAR. Geology, 43(8): 743–746, doi:10.1130/G36678.1.

Schaefer, L., Lu, Z. and Oommen, T., 2016. Post-Eruption Deformation Processes Measured Using ALOS-1 and UAVSAR InSAR at Pacaya Volcano, Guatemala. Remote Sensing, 8(1): 73, doi:10.3390/rs8010073.

Schmincke, H.-U., 1982. Volcanic and chemical evolution of the Canary Islands. In: von Rad, U., Hinz, K., Sarnthein, M., Seibold, E. (Eds.), Geology of the Northwest African Continental Margin, pp. 273-301, doi:10.1007/978-3-642-68409-8_12.

Segall, P., Desmarais, E.K., Shelly, D., Miklius, A. and Cervelli, P., 2006. Earthquakes triggered by silent slip events on Kilauea volcano, Hawaii. Nature, 442(7098): 71–74, doi:10.1038/nature04938.

Shirzaei, M., Bürgmann, R., Foster, J., Walter, T.R. and Brooks, B.A., 2013. Aseismic deformation across the Hilina fault system, Hawaii, revealed by wavelet analysis of InSAR and GPS time series. Earth Planet. Sci. Lett., 376: 12–19, doi:10.1016/j.epsl.2013.06.011.

Siniscalchi, A., Tripaldi, S., Neri, M., Balasco, M., Romano, G., Ruch, J., Schiavone, D., 2012. Flank instability structure of Mt. Etna inferred by a magnetotelluric survey. J. Geophys. Res., 117(3): doi:10.1029/2011JB008657.

Solaro, G., Acocella, V., Pepe, S., Ruch, J., Neri, M., Sansosti E., 2010. Anatomy of an unstable volcano from InSAR: Multiple processes affecting flank instability at Mt. Etna, 1994–

2008. J. Geophys. Res., 115(B10): doi:10.1029/2009JB000820.
Staudacher, T., Peltier, A., 2016. Ground deformation at Piton de la Fournaise (La Réunion Island), a review from 20 years of GNSS monitoring. In: Bachèlery, P., Lénat, J.F., Di Muro, A., Michon, L. (Eds.), Active volcanoes of the Southwest Indian Ocean: Piton de la Fournaise and Karthala, pp. 139–170, doi:10.1007/978-3-642-31395-0_9.
Swanson, D.A., Duffield, W.A. and Fiske, R.S., 1976. Displacement of the south flank of Kilauea Volcano: the result of forceful intrusion of magma into the rift zones. U.S. Geol. Surv. Prof. Pap. 963, 39 pp.
Swanson, D.A., Rose, T.R., Mucek, A.E., Garcia, M.O., Fiske, R.S. and Mastin, L.G., 2014. Cycles of explosive and effusive eruptions at Kīlauea Volcano, Hawai‘i. Geology, 42(7): 631–634, doi:10.1130/G35701.1.
Tibaldi, A., 2001. Multiple sector collapses at Stromboli volcano, Italy: How they work. Bull. Volcanol., 63(2): 112–125, doi:10.1007/s004450100129.
Tibaldi, A., Groppelli, G., 2002. Volcano-tectonic activity along structures of the unstable NE flank of Mt. Etna (Italy) and their possible origin. J. Volcanol. Geotherm. Res., 115(3–4): 277–302, doi:10.1016/S0377-0273(01)00305-5..
Tilling, R.I. and Dvorak, J.J., 1993. Anatomy of a basaltic volcano. Nature, 363(6425): 125–133, doi:10.1038/363125a0.
Tinard, P., 2007. Caractérisation et modélisation des déplacements du sol associés à l'activité volcanique du Piton de la Fournaise, île de La Réunion, à partir de données interférométriques. Août 2003 – Avril 2007. PhD Thesis, Université de Clermont Ferrand, 334 pp.
Tridon, M., Cayol, V., Froger, J.L., Augier, A., Bachèlery, P., 2016, Inversion of coeval shear and normal stress of Piton de la Fournaise flank displacement. J. Geophys. Res., 121(11): 7846–7866, doi:10.1002/2016JB013330.
Urgeles, R., Canals, M., Baraza, J., Alonso, B., Masson, D., 1997. The most recent megalandslides of the Canary Islands: El Golfo debris avalanche and Canary debris flow, west El Hierro Island. J. Geophys. Res., 102(B9): 20,305–20,323, doi:10.1029/97JB00649.
Van Ark, E. and Lin, J., 2004. Time variation in igneous volume flux of the Hawaii-Emperor hot spot seamount chain. J. Geophys. Res., 109(B11): doi:10.1029/2003JB002949.
van Wyk de Vries, B. and Borgia, A., 1996. The role of basement in volcano deformation. In: McGuire, W.J., Jones, A.P., Newberg, J. (Eds.), Volcano Instability on the Earth and Other Planets. Geol. Soc. Lon. Sp. Pub., 110, pp. 95–110.
Villeneuve, N., Bachèlery, P., 2006. Revue de la typologie des éruptions au Piton de La Fournaise, processus et risques volcaniques associés. Cybergeo: Eur. J. Geogr, doi:10.4000/cybergeo.2536.
Villeneuve, N., Bachèlery, P., Kemp, J., 2014. La Réunion Island: A typical example of a basaltic shield volcano with rapid evolution. In: Fort, M., André, M.-F. (Eds.), Landscapes and Landforms of France, pp. 261–270, doi:10.1007/978-94-007-7022-5_25.
Walter, T.R., Troll, V.R., Cailleau, B., Belousov, A., Schmincke, H.U., Amelung, F. and Bogaard, P.v.d., 2005. Rift zone reorganization through flank instability in ocean island volcanoes: an example from Tenerife, Canary Islands. Bull. Volcanol., 67(4): 281–291, doi:10.1007/s00445-004-0352-z.
White, R. S., 1993. Melt production rates in mantle plumes. Philos. Trans. R. Soc. Lond. Ser. A, 342(1663): 137–153, doi:10.1098/rsta.1993.0010.

1514 Wolfe, C.J., Brooks, B.A., Foster, J.H. and Okubo, P.G., 2007. Microearthquake streaks and
1515 seismicity triggered by slow earthquakes on the mobile south flank of Kilauea Volcano,
1516 Hawai'i. Geophys. Res. Lett., 34(23): doi:10.1029/2007GL031625.
1517 Wright, T.L. and Klein, F.W., 2014. Two hundred years of magma transport and storage at
1518 Kilauea Volcano, Hawai'i, 1790–2008. U.S. Geol. Surv. Prof. Pap. 1806,
1519 doi:10.3133/pp1806.

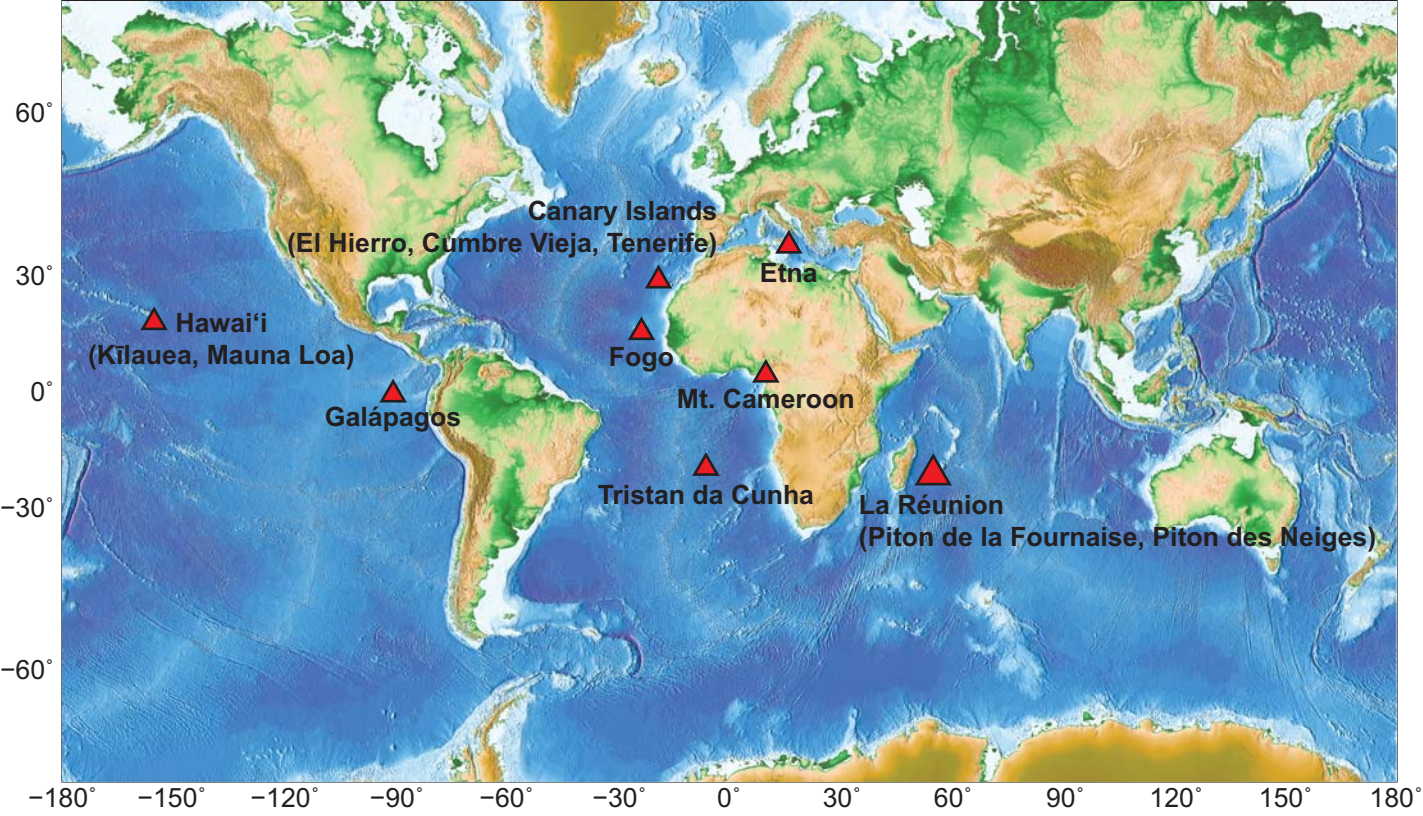
Canary Islands
(El Hierro, Cumbre Vieja, Tenerife)
Etna
Hawai'i
(Kīlauea, Mauna Loa)
Fogo
Mt. Cameroon
Galápagos
Tristan da Cunha
La Réunion
(Piton de la Fournaise, Piton des Neiges)
60°
30°
0°
−30°
−60°
−180°
−150°
−120°
−90°
−60°
−30°
0°
30°
60°
90°
120°
150°
180°

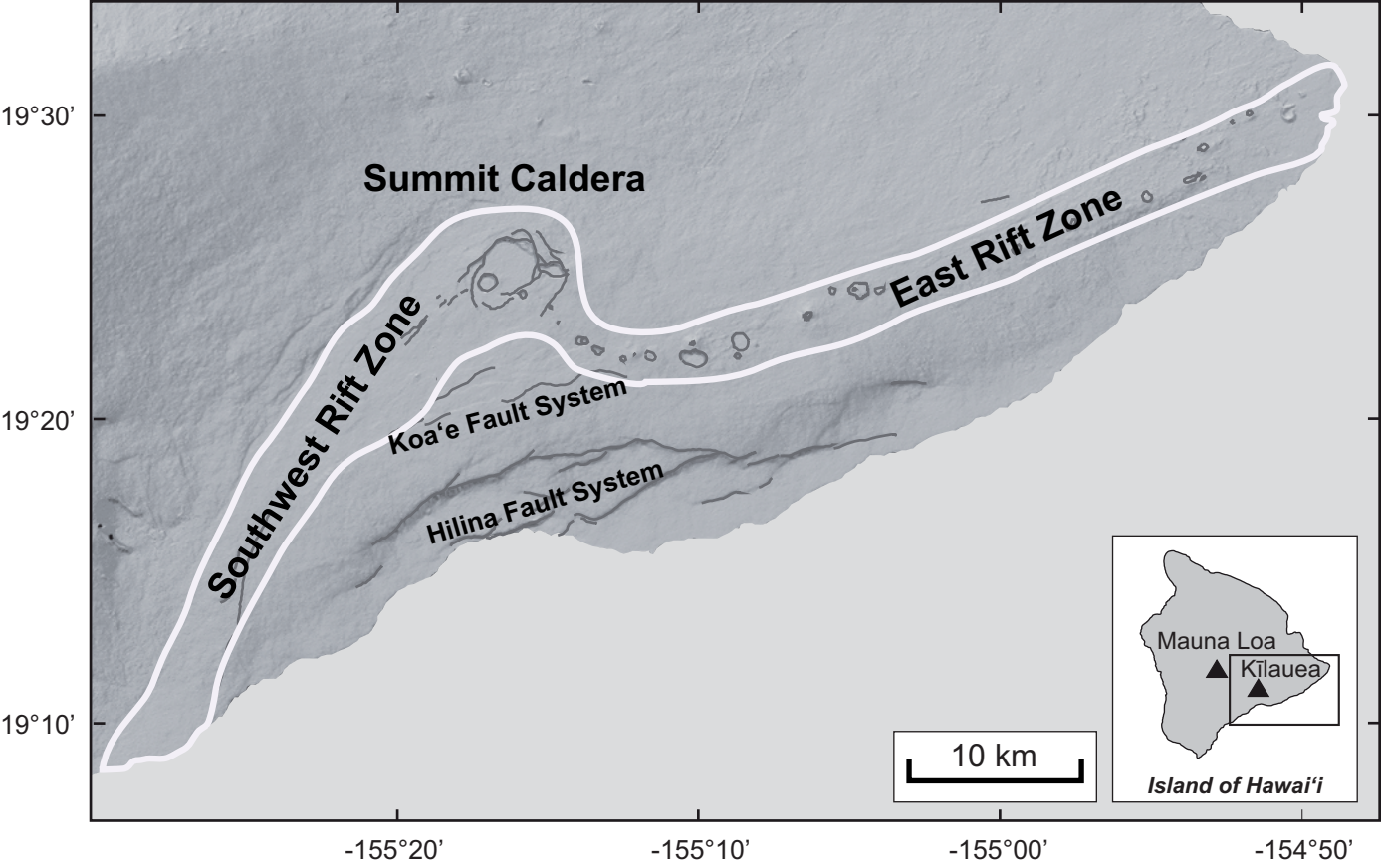
Summit Caldera
East Rift Zone
Southwest Rift Zone
Koa'e Fault System
Hilina Fault System
19°30'
19°20'
19°10'
-155°20'
-155°10'
-155°00'
-154°50'
10 km
Mauna Loa
Kīlauea
Island of Hawai'i

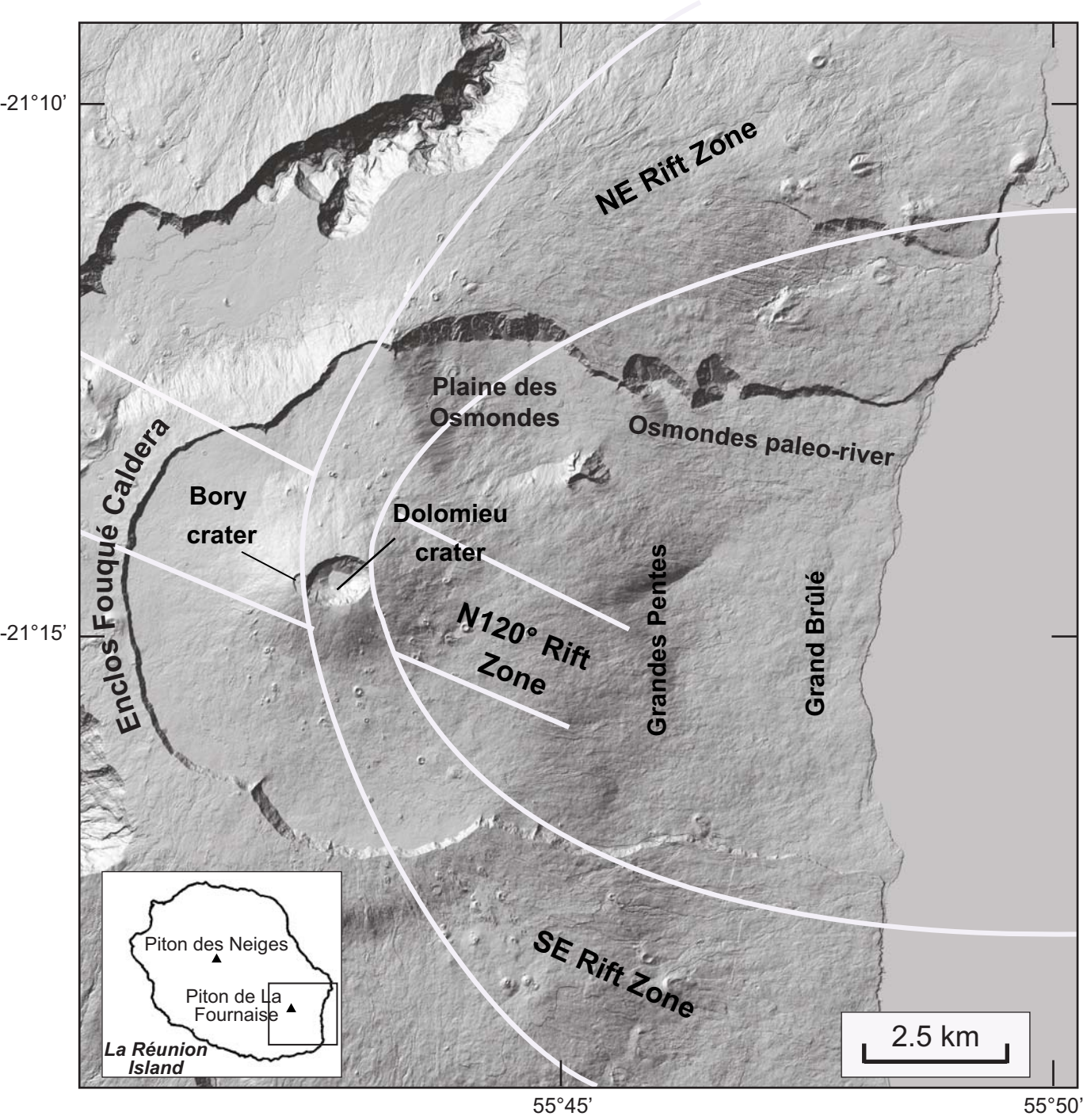
-21°10'
-21°15'
55°45'
55°50'
NE Rift Zone
Plaine des Osmondes
Osmondes paleo-river
Enclos Fouqué Caldera
Bory crater
Dolomieu crater
N120° Rift Zone
Grandes Pentes
Grand Brûlé
SE Rift Zone
Piton des Neiges
Piton de La Fournaise
La Réunion Island
2.5 km

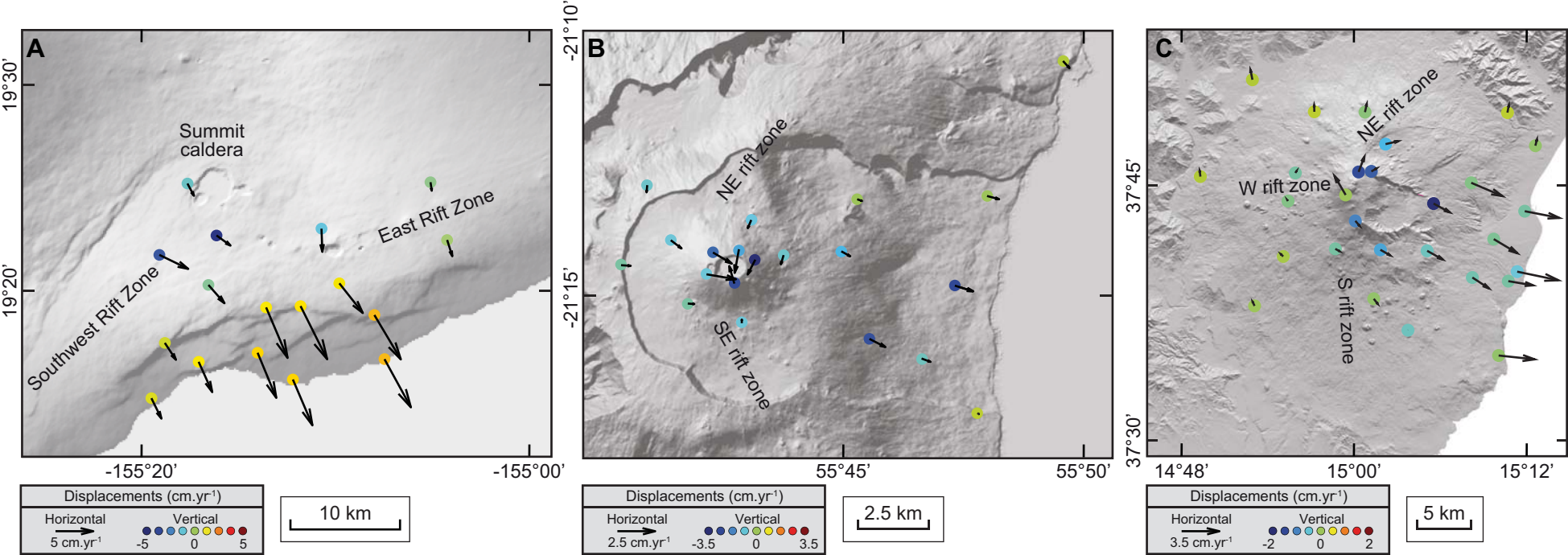
A
Summit caldera
East Rift Zone
Southwest Rift Zone
19°30'
19°20'
-155°20'
-155°00'
Displacements (cm.yr-1)
Horizontal
5 cm.yr-1
Vertical
-5
0
5
10 km
B
NE rift zone
SE rift zone
-21°10'
-21°15'
55°45'
55°50'
Displacements (cm.yr-1)
Horizontal
2.5 cm.yr-1
Vertical
-3.5
0
3.5
2.5 km
C
NE rift zone
W rift zone
S rift zone
37°45'
37°30'
14°48'
15°00'
15°12'
Displacements (cm.yr-1)
Horizontal
3.5 cm.yr-1
Vertical
-2
0
2
5 km

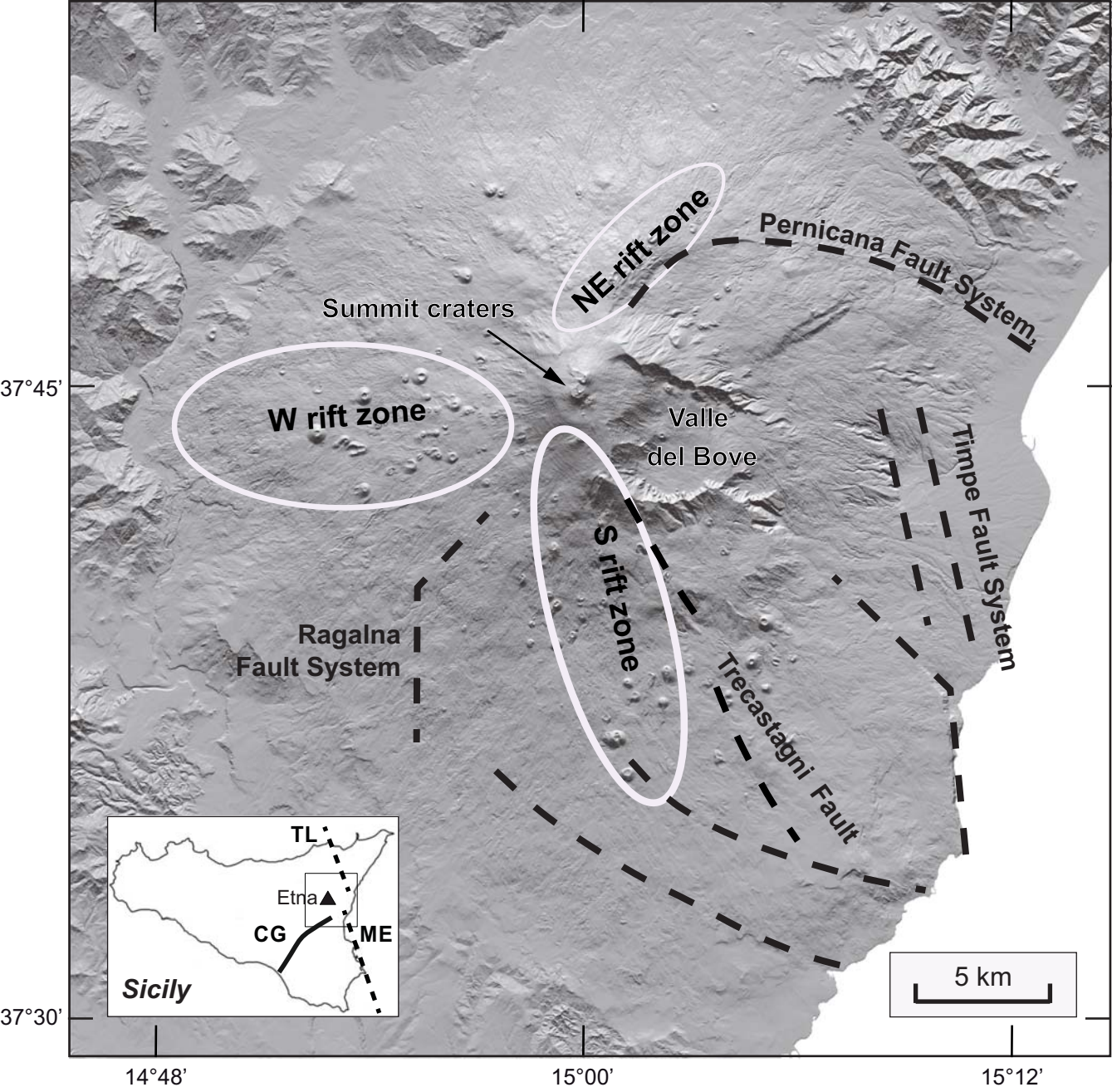
NE rift zone
Pernicana Fault System
Summit craters
W rift zone
Valle
del Bove
S rift zone
Timpe Fault System
Ragalna
Fault System
Trecastagni Fault
TL
Etna
CG
ME
Sicily
5 km
37°45'
37°30'
14°48'
15°00'
15°12'

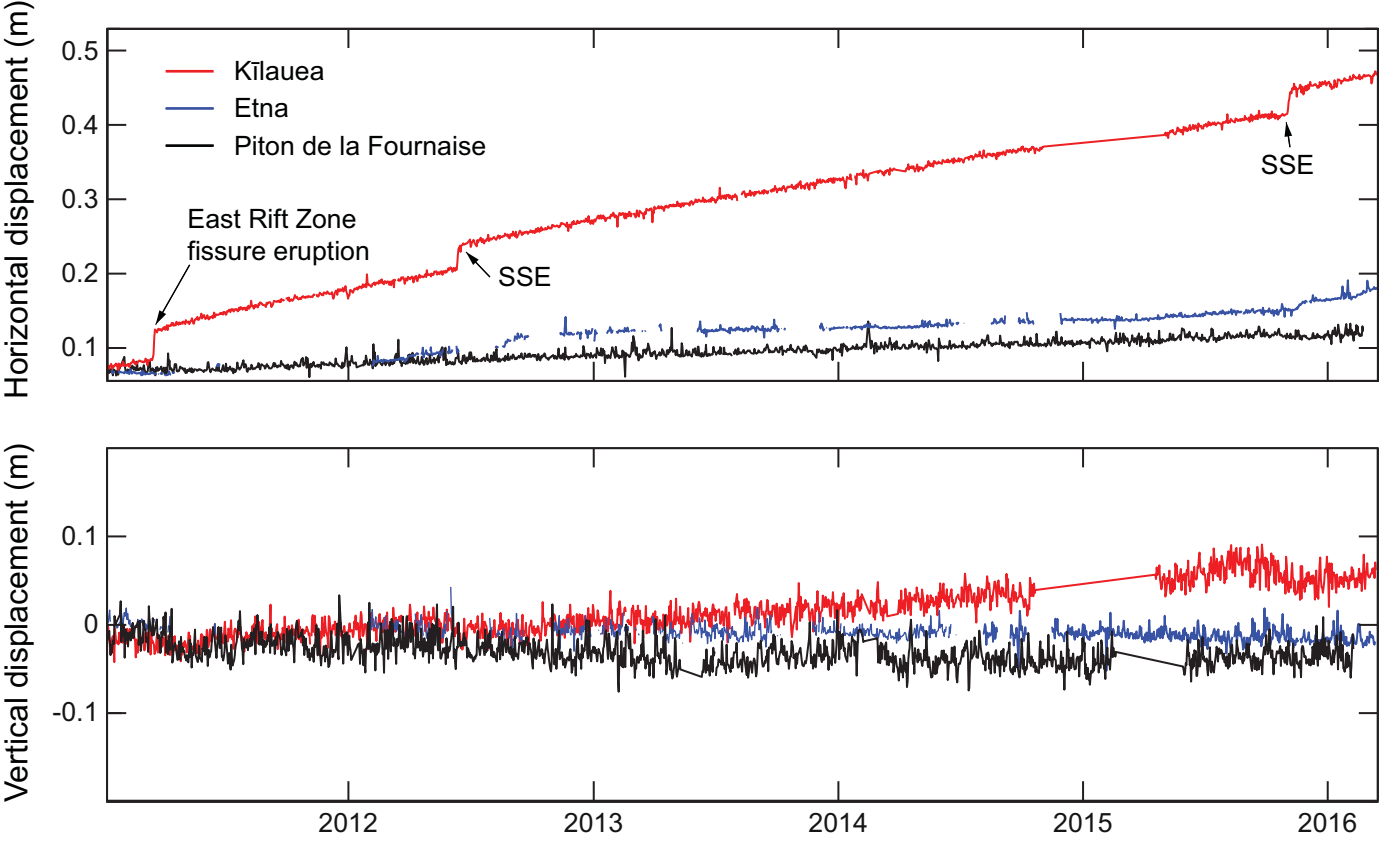
Horizontal displacement (m)
0.5
0.4
0.3
0.2
0.1
Kīlauea
Etna
Piton de la Fournaise
East Rift Zone
fissure eruption
SSE
SSE
Vertical displacement (m)
0.1
0
-0.1
2012
2013
2014
2015
2016

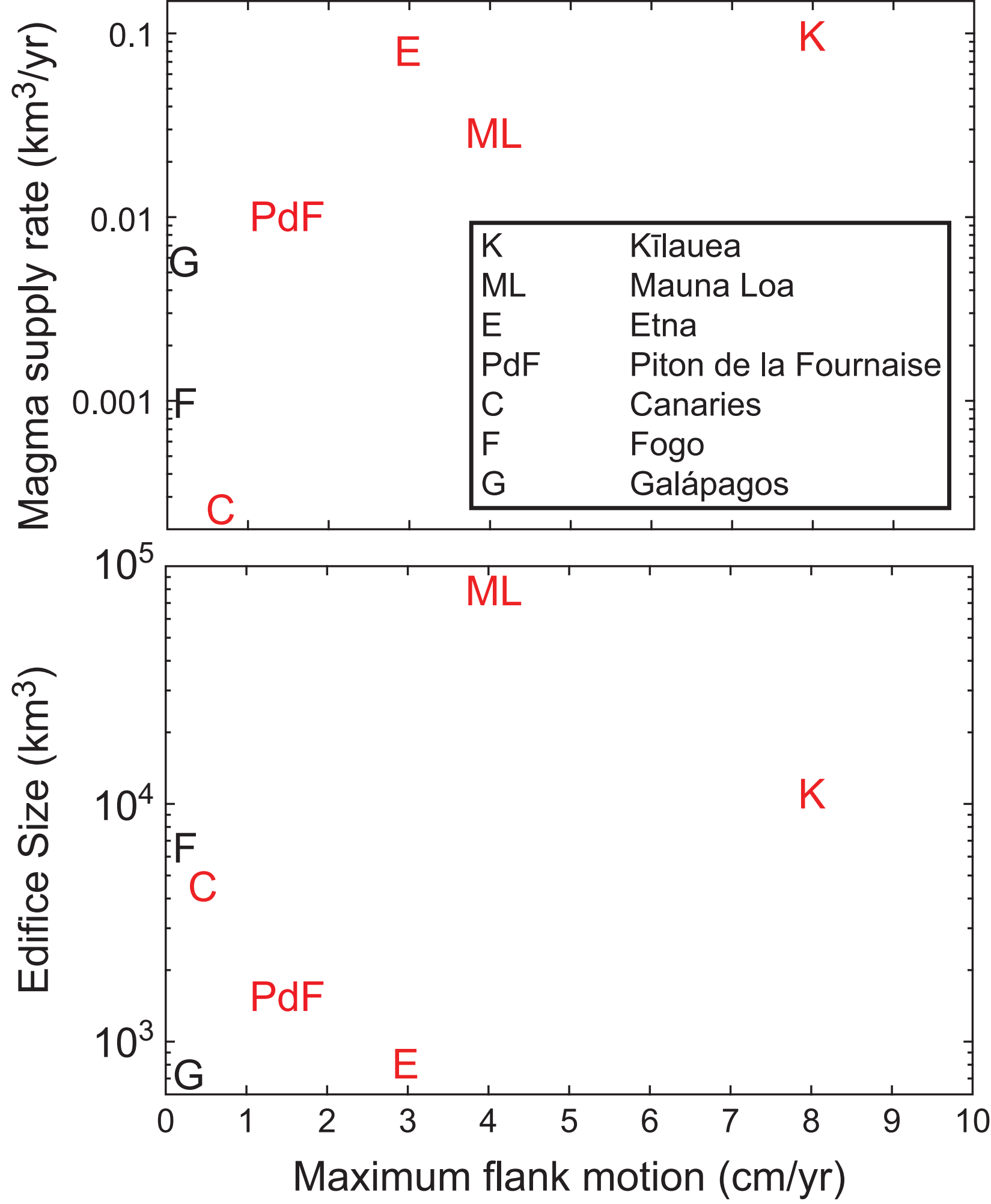
Magma supply rate (km3/yr)
0.1
0.01
0.001
E
K
ML
PdF
G
F
C
K Kīlauea
ML Mauna Loa
E Etna
PdF Piton de la Fournaise
C Canaries
F Fogo
G Galápagos
Edifice Size (km3)
10^5
10^4
10^3
ML
K
F
C
PdF
G
E
0
1
2
3
4
5
6
7
8
9
10
Maximum flank motion (cm/yr)

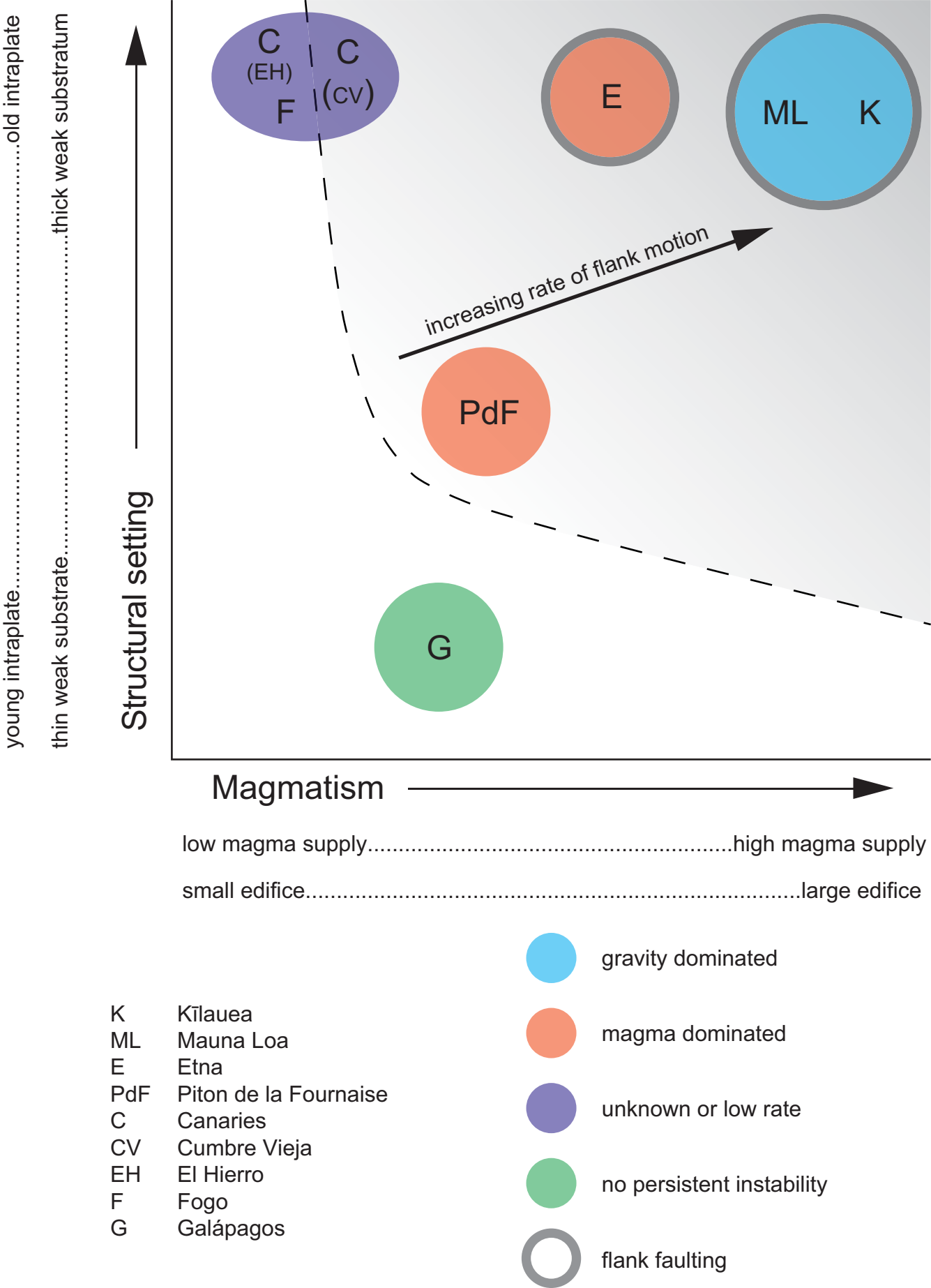
young intraplate.....old intraplate
thin weak substrate.....thick weak substratum
Structural setting
C
(EH)
F
C
(CV)
E
ML
K
increasing rate of flank motion
PdF
G
Magmatism
low magma supply.....high magma supply
small edifice.....large edifice
K Kīlauea
ML Mauna Loa
E Etna
PdF Piton de la Fournaise
C Canaries
CV Cumbre Vieja
EH El Hierro
F Fogo
G Galápagos
gravity dominated
magma dominated
unknown or low rate
no persistent instability
flank faulting